JOURNAL OF PETROLOGY | VOLUME 45 | NUMBER 3 | PAGES 507–530 | 2004 | DOI: 10.1093/petrology/egg092

The Shape and Volume of the Skaergaard Intrusion, Greenland: Implications for Mass Balance and Bulk Composition

TROELS F. D. NIELSEN*

GEOLOGICAL SURVEY OF DENMARK AND GREENLAND AND DANISH LITHOSPHERE CENTRE, ØSTER VOLDGADE 10, DK-1350, COPENHAGEN K, DENMARK

RECEIVED JULY 12, 2002; ACCEPTED JULY 31, 2003

Re-examination of the Skaergaard intrusion in the context of its regional setting, combined with new data from exploration drilling, has resulted in a revised structural model for the intrusion. It is modelled as an irregular box, c. *11 km from north to south, up to 8 km from east to west, and 3·4–4 km from the lower to the upper contact. The walls of the intrusion are inferred to follow pre-existing and penecontemporaneous steep faults, and the floor and roof seem largely controlled by bedding planes in the host sediments and lavas, similar to regional sills. The suggested shape and volume are in agreement with published gravimetric modelling. Crystallization along all margins of the intrusion concentrated the evolving melt in the upper, central part of the intrusion, best visualized as an 'onion-skin' structure inside the box. The total volume is estimated to* c. *280 ± 23 km^3, of which 13·7% are referred to the Upper Border Series (UBS), 16·4% to the Marginal Border Series (MBS) and 69·9% to the Layered Series (LS). In the LS, the Lower Zone (LZ) is estimated to constitute 66·8%, the Middle Zone (MZ) 13·5% and the Upper Zone (UZ) 19·7%. The new volume relationships provide a mass balance estimate of the major and trace element bulk composition of the intrusion. The parental magma to the Skaergaard intrusion is similar to high-Ti East Greenland tholeiitic plateau basalts with Mg number* c. *0.45. The intrusion represents the solidification of contemporary plateau basalt magma trapped and crystallized under closed-system conditions in a crustal reservoir at the developing East Greenland continental margin.*

KEY WORDS: *bulk composition; emplacement; mass proportions; Skaergaard intrusion; structure*

INTRODUCTION

The Tertiary Skaergaard intrusion, southern East Greenland (Wager & Deer, 1939; McBirney, 1996; Irvine *et al*., 1998), has for decades been the testing ground for models of magmatic differentiation. Despite an abundance of field data, the shape of the magma chamber, its internal structure and the volume relations in the intrusion remain largely hypothetical and inadequate for mass balance calculations and petrogenetic modelling. The need for detailed modelling of the shape and volume of the intrusion as a whole, and of lithological zones in the intrusion, has increased over the last decade, not only for purely academic reasons, but also as a consequence of the identification of major precious metal deposits within the intrusion (e.g. Nielsen & Schønwandt, 1990; Bird *et al*., 1991; Andersen *et al*., 1998). The intrusion hosts a potential world-class deposit with >20 million ounces of PGE (mainly Pd) and Au in a 5 m wide stratiform horizon (Nielsen, 2001).

Wager & Deer (1939) proposed the existence of a deep funnel-like magma chamber and presented mass balance estimates that suggested the presence of an unexposed sequence of early gabbros (the Hidden Zone, HZ) representing 60–70% of the initial volume of the intrusion (Wager & Brown, 1968). Mass balances based on the data of Wager (1960) and Wager & Brown (1968) led Chayes (1970) to suggest an even larger volume of unexposed cumulates.

The very large proportion of unexposed gabbros has, however, been questioned in a number of investigations. These include investigation of the Zr/Hf in the

*Telephone: (+45) 381 42224. Fax: (+45) 381 42220. E-mail: tfn@geus.dk

gabbros of the Skaergaard intrusion (Brooks, 1969), a structural model based on gravity data (Blank & Gettings, 1973; Norton *et al*., 1984), and the systematics in the mineral chemistry of plagioclase from a research drill core in the Lower Zone of the intrusion (Maaløe, 1976). In all of these investigations the volume of unexposed gabbros is considered to be much smaller, probably of the order of 10–20%.

The emplacement of the intrusion was suggested by Irvine (1992) and Irvine *et al*. (1998), at least in part, to be controlled by faults in the Lower Tertiary coast-parallel flexure of the East Greenland rifted volcanic margin (Nielsen & Brooks, 1981). This is in agreement with the intrusion being contemporaneous with regional faulting and deformation (e.g. Nielsen & Brooks, 1981; Pedersen *et al*., 1997), emplacement of large sill complexes (Storey *et al*., 1996; Tegner *et al*., 1998) and extrusion of flood basalts (Brooks & Nielsen, 1982*a*, 1982*b*; Nielsen, 1987).

Inspired by the work of Irvine (1992) and Irvine *et al*. (1998), the shape of the Skaergaard magma chamber is here suggested to be controlled by pre-existing and penecontemporaneous, steep faults and the bedding planes in the Tertiary country rocks. This allows the reconstruction of the original shape of the magma chamber and calculation of the bulk volume of the intrusion. The internal structure and volume relationships between lithological zones and subzones are evaluated using constraints from 34 exploration drill cores of up to 1100 m length through the upper part of the Layered Series (LS) of the intrusion. The cores were drilled in 1989 and 1990 by Platinova Resources Ltd. (Watts, Griffis & McOuat, 1991). An estimate for the bulk composition of the intrusion can, in turn, be calculated from the mass balances and average compositions of the lithological zones (McBirney, 1989*a*, 1996).

Although the calculations cannot give a unique estimate for the parental magma of the intrusion, a comparison between the calculated composition and the compositions of the chilled margin of the intrusion and contemporaneous tholeiitic lavas and dykes serves as a test for the suggested structure and the calculated bulk composition.

THE SKAERGAARD INTRUSION

The Skaergaard intrusion (Fig. 1) was made famous by the works of L. R. Wager and colleagues (e.g. Wager & Deer, 1939; Wager & Brown, 1968), and has, because of its excellent exposures, been a natural laboratory for the study of magmatic differentiation, crystallization and solidification processes, and the evolution of tholeiitic magma stored in crustal reservoirs (e.g. Wager & Deer, 1939; Wager & Brown, 1968; McBirney & Noyes, 1979; Hunter & Sparks, 1987; Toplis & Carroll, 1995; McBirney, 1996; Thy *et al*., 1996; Irvine *et al*., 1998).

The Skaergaard intrusion was emplaced *c*. 55 Myr ago (Brooks & Gleadow, 1977; Hirschman *et al*., 1997) in the lower part of the accumulating Tertiary East Greenland plateau basalts during continental break-up in the North Atlantic (Nielsen, 1975; Larsen *et al*., 1989; Tegner *et al*., 1998). The magmatism along the East Greenland margin lasted from 61 to 13 Ma (Storey *et al*., 1996; Tegner *et al*., 1998).

It is generally accepted that the Skaergaard magma chamber was filled in a single event and fractionated under generally closed-system conditions (e.g. Wager & Brown, 1968; McBirney, 1996*a*; Irvine *et al*., 1998). It has, however, been argued that an evolved silicic melt may have escaped the intrusion (Hunter & Sparks, 1987), a conclusion refuted by Brooks & Nielsen (1990), McBirney & Naslund (1990) and Morse (1990).

In plan view the intrusion is an irregular, 11 km × 8 km, oval-shaped body (Fig. 1). Much of the contact is, however, not exposed, and thus the suggested shape for the intrusion is an interpretation. Almost all exposed contacts of the intrusion are steep (see McBirney, 1989*b*; Irvine *et al*., 1998). In the southern part of the intrusion the roof contact is preserved in a small area, but the lower contact (or floor) of the intrusion is nowhere exposed. No drill cores have intersected the lower contact. Post-solidification subsidence of the East Greenland continental margin has resulted in the seaward tilting of the intrusion, so that structures that originally were horizontal now dip between 10 and 20° SSE.

The internal structure of the intrusion results from crystallization processes. It is traditionally divided into three series: the Layered Series (LS), the Marginal Border Series (MBS) and the Upper Border Series (UBS) (Fig. 2). The LS accumulated up from the floor, the UBS down from the roof and the MBS in from the walls of magma chamber (Fig. 2). The LS and UBS meet *c*. 600 m below the roof of the intrusion in the Sandwich Horizon (SH). All three series were assumed by Wager & Deer (1939), and most subsequent investigators, to have crystallized from the same parental magma. Differences in mineral assemblage and mineral chemistry in the gabbros are believed to reflect differences in the crystallization conditions in different parts of the magma chamber. Hoover (1989*a*), however, suggested that the magma separated during cooling into two compartments: a UBS chamber and an LS chamber. For the present purpose the traditional view that all three zones crystallized from the same liquid has been adopted.

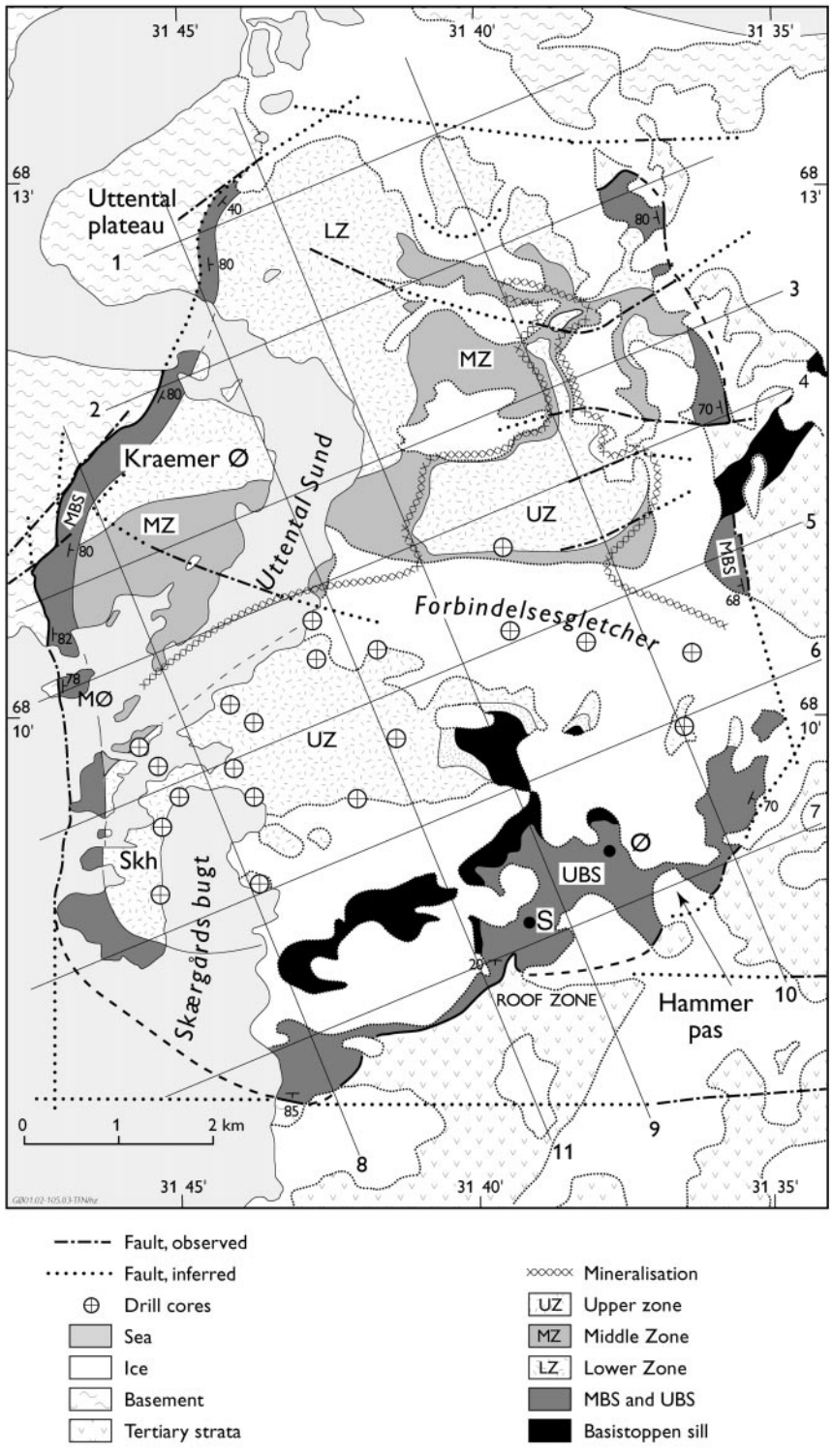

Fig. 1. Geological sketch map of the Skaergaard intrusion based on McBirney (1989*b*). Strike and dip of marginal gabbros and faults within the intrusion are from McBirney (1989*b*). Observed and suggested faults along the margins are in part from Irvine *et al.* (1998) and in part from this work. The main lithological series and zones in the intrusion are shown as indicated in the legend (see Fig. 2 for further details). The location of drill cores is defined by the collar positions. The mineralization in the intrusion is hosted in the Triple Group consisting of macrorhythmic layers in ferrodiorite in the upper part of the Middle Zone (MZ). The Basistoppen Sill and the Vandfaldsdalen Macrodyke on the eastern margin of the intrusion are shown in black. The grid shows the position of cross-sections (sections 1–11) in Figs 7–9 and in Electronic Appendices EA1.1 to EA1.3. S, Sydtoppen; Ø, Østtoppen; MØ, Mellemø; Skh, Skærgårdshalvø.

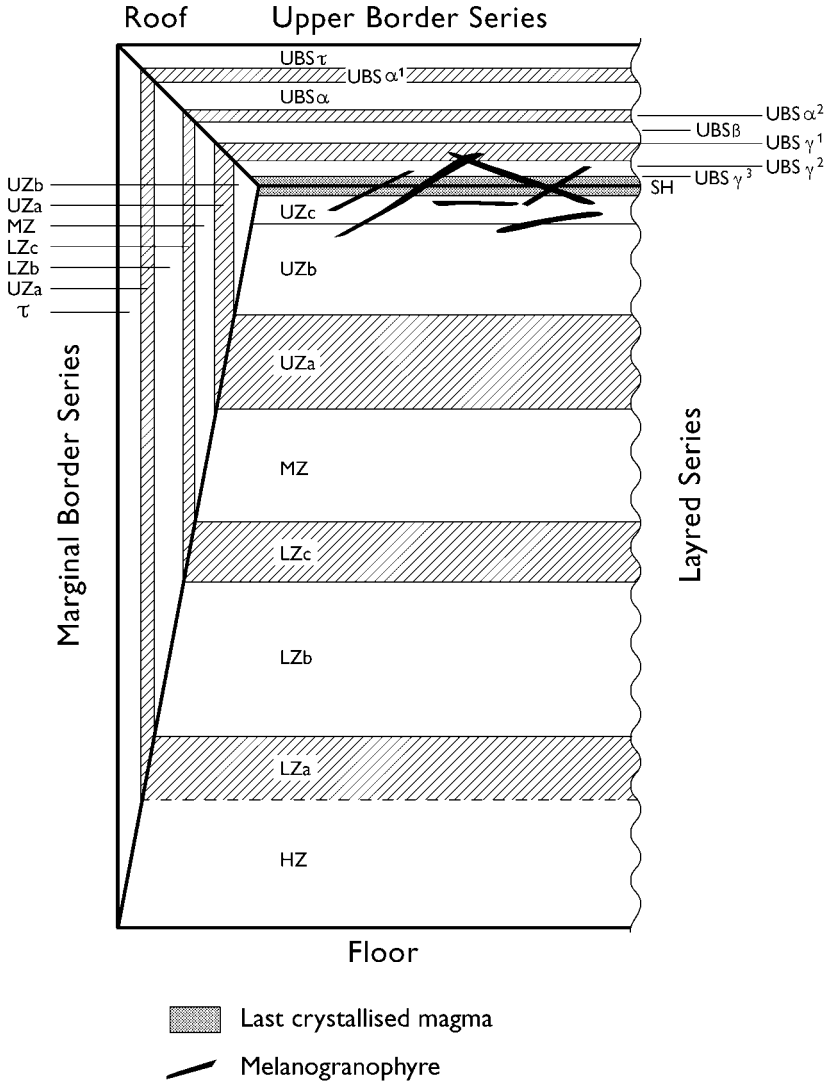

Fig. 2. Schematic section of the Skaergaard magma chamber with lithological subdivisions (after McBirney, 1989*b*; Irvine *et al*., 1998). Every second subdivision has been shaded to facilitate correlation from the Layered Series (LS) to the Marginal Border Series (MBS) and the Upper Border Series (UBS). Further details have been given by McBirney (1996*b*) and Irvine *et al*. (1998). The last melt to crystallize in the intrusion is identified as the grey area on either side of the Sandwich Horizon (SH). Following McBirney (1996), the Sandwich Horizon is a demarcation zone between lithologies accumulated up from the floor and down from the roof of the intrusion. The last crystallized lithologies above and below the SH are shown in grey. Melanogranophyres are shown schematically. Not to scale.

The LS is divided into four zones [see Wager & Deer (1939) and Wager & Brown (1968), and, for more recent summaries, McBirney (1996) and Irvine *et al*. (1998)]: the unexposed Hidden Zone (HZ), the Lower Zone (LZ, with subzones a–c), the Middle Zone (MZ) and the Upper Zone (UZ, with subzones a–c), based on the observed assemblages of cumulus phases. Detailed descriptions of the lithological subdivisions have been given by Wager & Brown (1968), McBirney (1996) and Irvine *et al*. (1998).

The MBS and the UBS show cumulus phase chemistries in general harmony with those of the LS (Naslund, 1984; Hoover, 1989*a*), and the cumulate zones in all three main units (LS, UBS and MBS) can be correlated (Fig. 2). There are systematic bulk composition differences between the three series (e.g. Naslund, 1984; McBirney, 1989*a*). The most noticeable is that the average FeO^* and TiO_2 concentrations in the UBS are much lower than in the MBS and the LS. This is probably the result of gravitational settling of Fe- and Ti-rich minerals or melts from the upper part of the magma chamber (see, e.g. Naslund, 1984; McBirney, 1989*a*; Irvine *et al*., 1998).

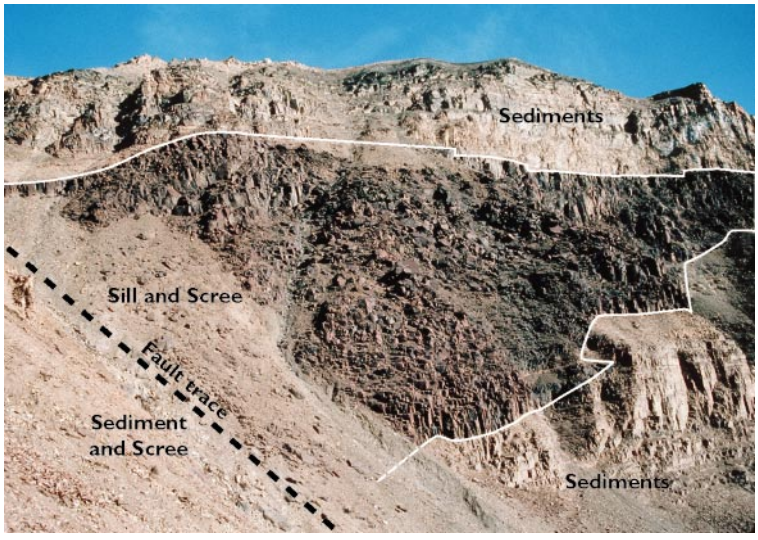

Fig. 3. Damming of magma at a fault in the sedimentary mountains, NE of the Skaergaard intrusion. The sill belongs to a sill province with an integrated total thickness of *c.* 1000 m (Gisselø, 2000). The sills intrude the Cretaceous to Lower Tertiary sediments of the Kangerlussuaq Basin (Larsen *et al.*, 2001). They are penecontemporaneous with the Skaergaard intrusion. As suggested for the Skaergaard intrusion, the floor subsided to make room for the magma. The height of the face is *c.* 500 m. Interpretation of field relations and photograph by P. Gisselø (Gisselø, 2000).

REINTERPRETATION OF THE STRUCTURE OF THE SKAERGAARD INTRUSION

Contact relations

Irvine (1992) and Irvine *et al.* (1998) described the fault-controlled western, southern and eastern contacts of the Skaergaard intrusion. The contacts are chilled to the host rocks, which suggests that the intrusion exploited pre-existing or contemporaneous fault planes during emplacement. The magma was dammed by fault planes. Such damming of magma at fault planes is common in the large sill province in the areas to the east and NE of Skaergaard (Fig. 3, and Gisselø, 2000).

Elevated initial strontium isotope ratios (Stewart & DePaolo, 1990), xenoliths of host rocks (e.g. Irvine *et al.*, 1998), and the formation of sulphide concentration in the marginal gabbros (Wager *et al.*, 1957) suggest thermal erosion of the fault planes during the emplacement of the intrusion. It is thus mostly not possible to see the fault planes that shaped the intrusion, unless they are exposed in the host rocks outside the perimeter of the intrusion.

The western, southern and eastern contacts

Following Irvine *et al.* (1998), the present model assumes that the western contact is steep, broadly north–south, and controlled by pre-existing or syn-emplacement faults. This is illustrated on Kraemer Ø (Figs 1 and 4). From the south shore of Kraemer Ø the contact is north–south trending, steep (slightly east dipping) and irregular. About 800 m inland the contact shows an abrupt change to a NE–SW trend parallel to a fault zone in the basement gneisses [see also Hoover (1989*a*, fig. 7)]. At 300 m further NE the contact abruptly returns to the north–south trend for 200 m, followed by a NNE–SSW-trending and steep contact to the northern shore at Uttental Sund. North–south structural elements, such as the contemporaneous Skaergaard-like dykes (Brooks & Nielsen, 1978, 1990), are common on Kraemer Ø and the Uttental Plateau. NE–SW segments of the contact are parallel to post-Skaergaard dyke swarms (Fig. 3; Nielsen, 1978; Irvine *et al.*, 1998, fig. 1) and the fabrics in the host gneisses (Kays *et al.*, 1989). The field observations indicate that the chilled margin has not been subjected to faulting. All along the western margin the magma seems to have exploited pre-existing structures (see Hoover, 1989*a*; Irvine *et al.*, 1998). Minor movement continued along some fault planes after the emplacement of the intrusion. NE–SW and east–west lineaments and minor shear zones can now be followed as valleys inside the intrusion (Fig. 4).

The western contact is traditionally, and on the basis of the trajectories of internal zone boundaries in the MBS on Skærgårdshalvø (Skh, Fig. 1), suggested to curve through 90° into the southern east–west contact. However, the SW 'corner' of the intrusion is not exposed (Fig. 1). As discussed below, it is just as likely that the north–south-trending western contact continues to a near-perpendicular intersection with the fault-controlled east–west-trending southern contact (Fig. 1). The southern contact illustrates the transition

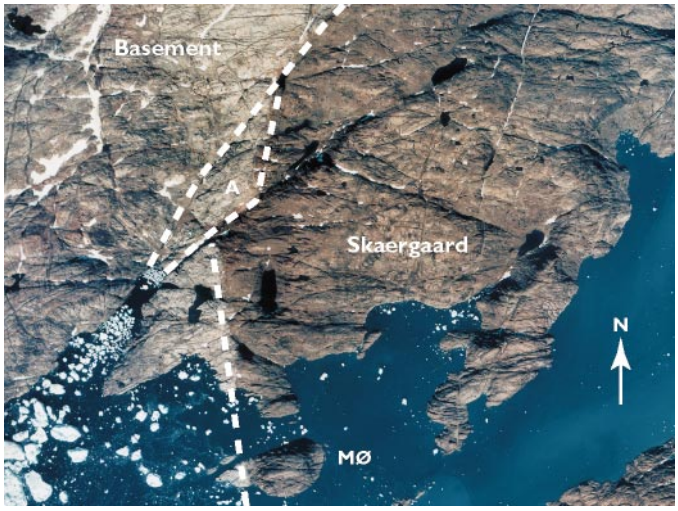

Fig. 4. Detail of aerial photograph of the western margin of the Skaergaard intrusion on Kraemer Ø (see Fig. 1). Aerial photograph was provided by A. R. McBirney. The field of view is *c.* 3·5 km from east to west and 2·5 km from north to south. The colours have been enhanced. The contact between the brown gabbros of the Skaergaard intrusion and the grey to cream Precambrian gneisses with dark amphibolitic enclaves is fault controlled. The fault zones along the margin of the intrusion (see text) can often be followed into the surrounding basement gneisses, where they occur as shear and fault zones. They can also be followed into the gabbros of the intrusion, where they form valleys along shear zones with little or no displacement. The characteristic chessboard pattern in the brown gabbros of the intrusion is caused by NNE–SSW-trending Skaergaard-like dykes (Brooks & Nielsen, 1978, 1990) and broadly east–west shear and fault zones parallel to the coast-parallel flexure (Nielsen & Brooks, 1981). Some of the east–west-oriented zones host post-Skaergaard mafic dykes (see Nielsen, 1978).

from a steep, fault-controlled southern wall of the intrusion into the bedding-controlled, south-dipping roof (see, e.g. Irvine, 1987; Irvine *et al*., 1998). Inland from the shore of Skaergaard Bugt the east–west contact is steep, but shallows 500 m inland to follow the contours to the southern flank of Sydtoppen. In Sydtoppen, the roof contact dips 15–20°S in broad agreement with the regional dip of the host lavas and large sill complexes to the south and east of the intrusion (Nielsen & Brooks, 1981; Nielsen *et al*., 1981; McBirney, 1989*b*; Irvine *et al*., 1998).

The trend of the contact at the SE corner of the intrusion remains largely guesswork, because of the extensive ice cover. South of Hammer Pas (Fig. 1) the east–west southern contact is traditionally suggested to 'swing' to a NNE trend. It is, however, nowhere exposed and could, by analogy with the field relations on Kraemer Ø, be a result of a combination of fault planes. In the Hammer Pas area (Fig. 1), the contact appears to trend NNE–SSW parallel to the Mikis Fjord Macrodyke, which is located east of the Skaergaard intrusion (outside the area in Fig. 1; see White *et al*., 1989; Blickert-Toft *et al*., 1992; Lesher *et al*., 1993). From Hammer Pas to the NE corner of the intrusion the contact is steep, broadly north–south and, as suggested by Irvine *et al*. (1998), fault controlled.

The northern contact

Exposures of the northern contact are very limited. The extent of the intrusion to the north is a key issue in modelling of the shape of the intrusion. At the NW corner of the intrusion on Uttental Plateau the contact dips *c.* 40° SE. This shallow dip is here interpreted as the dip of the contact close to the intersection between the walls and floor of the intrusion. Maaløe (1976) investigated a research drill core *c.* 1·5 km SSE of the NW corner. He estimated the depth to the south-dipping floor of the intrusion to be, perhaps, 850 m. This would suggest that the floor of the intrusion would surface close the most northerly exposures of Skaergaard gabbros in agreement with the interpretation of the shallow dip of the contact at the NW corner. Proximity to the base of the northern wall of the intrusion is also supported by the limited width of the MBS at the NW corner (see, e.g. Irvine *et al*., 1998).

The recent recession of glaciers and perennial snowfields has resulted in a limited exposure of the northern contact from the NW corner and eastward. As observed from the air, the contact is steep, trends 80° and is parallel to the fault zone that has faulted the sediments on the NE corner of the intrusion (see McBirney, 1989*b*). This fault zone can be followed more than 50 km to the east (Nielsen, 1975, fault number 2; Nielsen *et al*., 1981).

No field observations indicate that the Skaergaard intrusion ever extended beyond this northern fault zone and no data support the extrapolation of the Skaergaard gabbros into the air to the north of their present exposures. A northern, steep, and fault-controlled wall of the magma chamber is assumed in

the modelling below to be located adjacent to the most northerly exposures of Skaergaard gabbros.

Roof and floor

Only a few observations can be used for the modelling of the lower and upper contacts of the intrusion. The shallow dip of the roof contact (Wager & Deer, 1939; Irvine, 1987; McBirney, 1989*b*; Fig. 1) in the Sydtoppen area suggests bedding control and analogy to the widespread sill intrusions of the region (e.g. Wager, 1947; Gisselø, 2000). The analogy to sill intrusions suggests that the floor (excluding possible roots) and the roof contacts are broadly co-planar.

Reconstructing the magma chamber and its internal structure

The box model

The available field observations do not at present allow detailed descriptions of the fault patterns that controlled the shape of the Skaergaard intrusion. However, the suggestions, descriptions and models given by Irvine *et al.* (1998) and above lead to the suggestion that most, if not all, steep contacts were controlled by pre-existing or syn-emplacement fault planes developed along faults, shear zones and lineaments in the host rocks. The consequence of this is that the intrusion should not be perceived as an oval body with smooth and curved contacts, but rather as an irregular rectangular fault-controlled body.

The oval shape of the magma chamber (e.g. Irvine *et al.*, 1998) appears in some areas to be inspired by the trajectories of internal boundaries between zones and subzones; for example, in the MBS exposed on Skærgårdshalvø at the SW 'corner' (Fig. 1). In a box-like magma chamber with an 'onion-skin' internal structure (see below) curved internal boundaries are to be expected. They are caused by the increased cooling rates at the corners of the box and especially at the SW 'corner', located close to the intersection between the roof and the western and southern walls of the magma chamber. Thus, the internal zone boundaries do not necessarily mirror the trends of the external contacts of the intrusion and cannot necessarily be used for the reconstruction of the shape of the intrusion. The SW 'corner' may be shaped by the near-perpendicular intersection of the near-vertical north–south- and east–west-oriented western and southern contacts. The geophysical model of Blank & Gettings (1973; see also Norton *et al.*, 1984) does not constrain the shape of the SW corner further (see below).

Based on the interpretation of the contacts as linear features, the intrusion becomes box-like (Fig. 5) with a somewhat irregular outline determined by the intersecting fault planes. The box would be *c.* 11 km north–south and up to 8 km east–west. The height of the box is estimated to increase from 3·4 to 4 km from north to south (see below).

The geophysical model of Blank & Gettings (1973) [see also Norton *et al.* (1984)] may provide a test for the suggested box model (Fig. 6). Norton *et al.* (1984) showed the Skaergaard intrusion as an inflated sill with sills extending out from the perimeter of the intrusion. In Fig. 6 the north–south section through the box model is superimposed on a north–south section through the 3-D geophysical model of Norton *et al.* (1984). It is important to note that no field evidence exists for the suggested sill extensions, and they are believed to be purely model-driven. As noted by Norton *et al.* (1984), two large pre-Skaergaard sills may cause the gravimetric anomalies south of the exposures of the intrusion (see McBirney, 1989*b*). Sill extensions to the north are difficult to prove or disprove. They would have been located above the present level of erosion. Thin sills in the sedimentary rocks and the volcanic rocks to the east of the intrusion could be related to Skaergaard, but no field observations can confirm their relationship to the intrusion. No sill-like extensions are observed to the west of the intrusion.

Blank & Gettings (1973) identified two plutonic roots or feeders for the intrusion [see also Norton *et al.* (1984)]. No field observations or information from drill cores relate to potential roots for the intrusion and the present model does not include estimates for volumes in such roots. Even though the gravimetric model suggests that intrusive material does exist below the intrusion, no data show that this material forms part of the intrusion. Dykes (Nielsen, 1978) and macrodykes, up to 500 m wide (Brooks & Nielsen, 1982*a*, 1982*b*; Rosing *et al.*, 1989; White *et al.*, 1989), occur throughout the region and may occur in the substratum of the intrusion. They would not, however, necessarily be part of the Skaergaard magma chamber. The anomalies that led to the geophysical modelling of the roots could also be caused by basaltic dykes (A. R. McBirney, personal communication, 2003). With the exclusion of the sill extensions and the root, the present box-like shape shows a reasonable approximation to the gravimetric model (Fig. 6).

The internal structure—cross-sections

Eleven cross-sections (Figs 7–9; see also Electronic Appendix 1, which may be downloaded from the *Journal of Petrology* website at www.petrology.oupjournals.org) have been constructed to give information on the total height of the suggested box-like magma chamber and its internal structure. The sections form the basis for the calculation of the volume relations and the mass

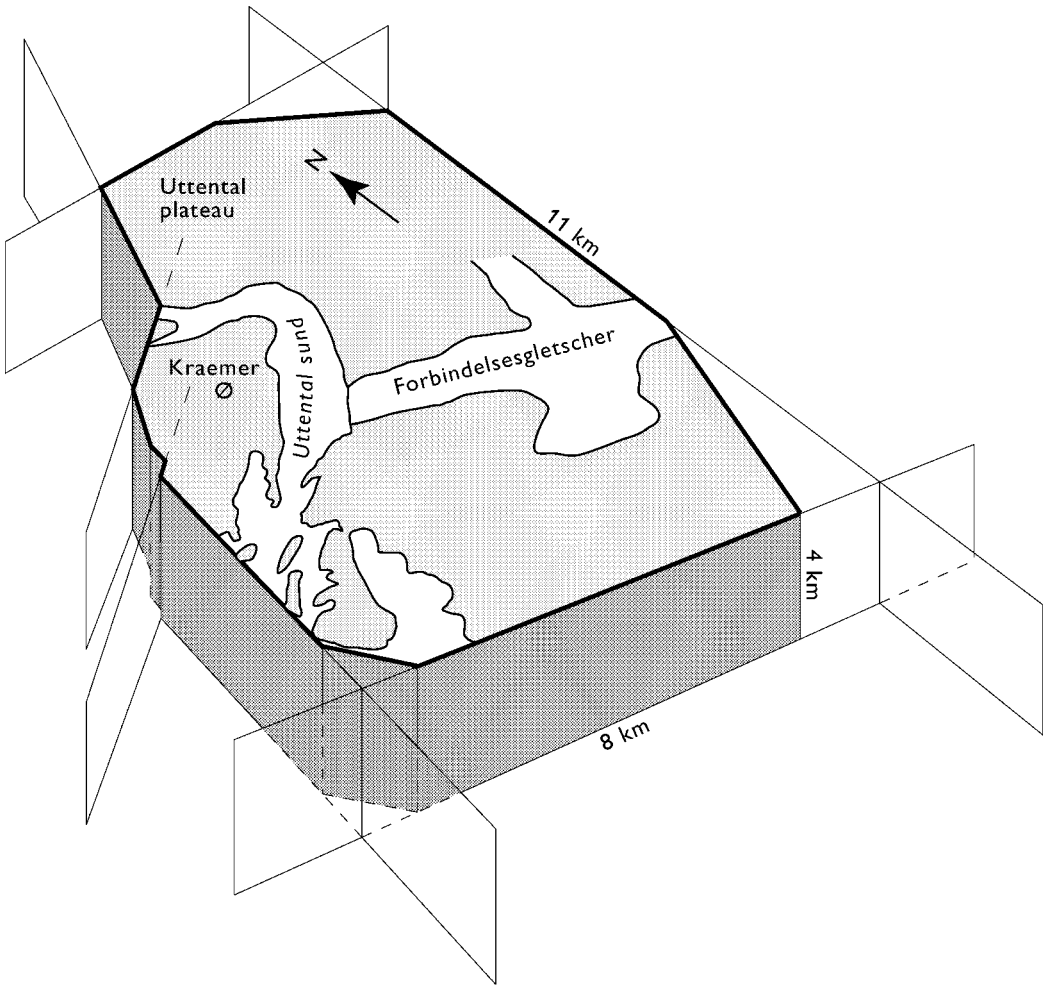

Fig. 5. Box model based on the outline of intrusion (Fig. 1) and the height of the magma chamber as constructed in Figs 9 and 10. The model is simplified. The coastline and margins of glaciers are superimposed on the box for orientation (see Fig. 1). The vertically ruled planes are the observed and suggested main fault planes that define the shape of the intrusion. They are extended beyond the margins of the intrusion for illustrative purposes, but they may not have been active faults beyond the perimeter of the intrusion.

proportions in the intrusion. The intrusion is tilted toward the SSE and the sections are accordingly oriented 340–160° and 70–250° (Fig. 1). The cross-sections were constructed assuming that:

(1) all walls of the intrusion are steep;
(2) the roof and floor contacts are sub-parallel, determined by the bedding planes in the Tertiary sediments and lavas and have dips similar to contemporaneous regional sills;
(3) the roof contact can be extrapolated northwards using the regional dip of the lavas and sedimentary rocks;
(4) the floor contact is sub-parallel to the roof contact and lies at a level just below exposures at the northern contact of the intrusion on Uttental Plateau (Fig. 1);
(5) the height of the magma chamber is slightly greater towards the coast (wedge-shaped magma chamber) as a result of the rotation of fault blocks in the coast-parallel flexure (see Nielsen & Brooks, 1981);
(6) the internal boundaries are smooth and regular, as they reflect isothermal structures; this is supported by the liquidus mineral composition contours presented by McBirney (1996);
(7) the MBS increases in width upwards, and continues into the UBS under the roof of the intrusion and downwards into equivalent LS zones along the floor of the intrusion [Fig. 2; see also interpretations given by McBirney (1989*b*, insert), Hoover (1989*a*, fig. 7) and Irvine *et al.* (1998)];

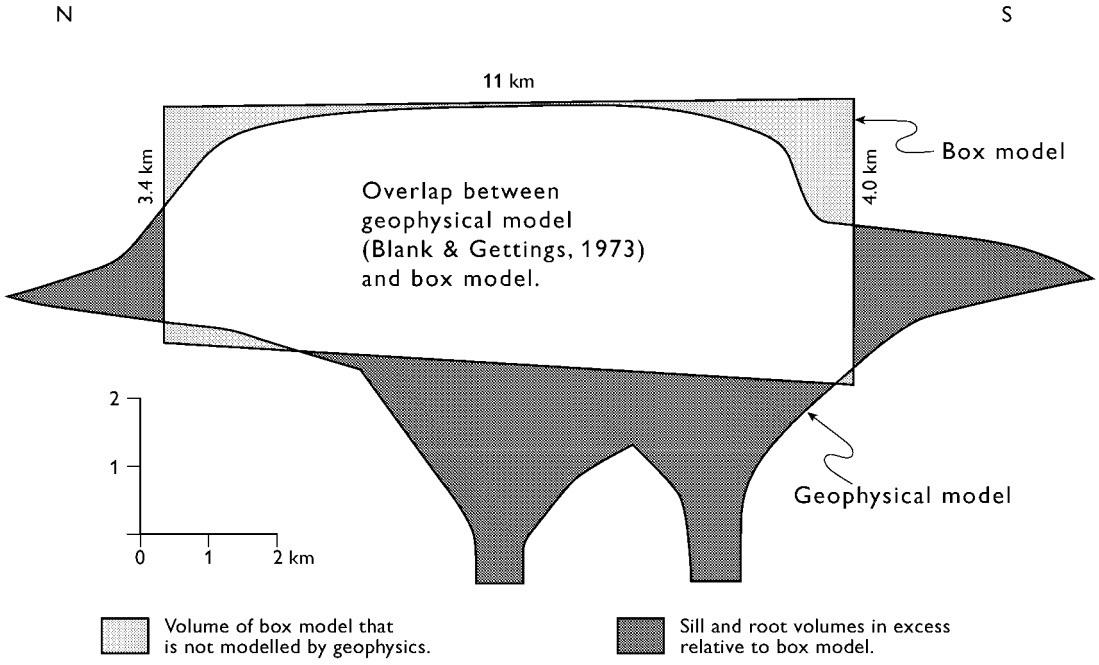

Fig. 6. North–south cross-section through the gravimetric model of the Skaergaard intrusion from Norton *et al.* (1984) [based on Blank & Gettings (1973)] with roots and sill extensions. A section of the box model in Fig. 5 is superimposed on the geophysical model. The 'excess' volumes in sill extensions and in the roots may not exist (see text for further details).

and using:

(1) exposed internal boundaries from McBirney (1989*b*);
(2) internal boundaries between the MZ and UZ from exploration drill cores (Turner, 1990; Watts, Griffis & McOuat, 1991).

Control points are projected onto the sections in accordance with the regional dip of the Tertiary stratigraphy. Three of the WSW–ENE sections are shown in Fig. 7 and the remaining sections can be found in Electronic Appendix 1. The most noticeable feature is the significant sagging of the boundaries in the centre of the intrusion. The sagging amounts to *c.* 700 m over a horizontal east–west distance of *c.* 7 km, equivalent to 10%.

NNW–SSE sections (Fig. 8) were constructed based on the WSW–ENE sections and surface and drill-core control points. Smoothing of internal boundaries in the NNW–SSE sections provides new secondary control points that have been transferred back to the first set of WSW–ENE cross-sections in an iterative process. The net result of the process is a smooth 'onion-skin' structure within the box-like magma chamber and the last solidified magma in the central and upper part of the intrusion (Fig. 9).

The last solidifying volume of magma in the present model is represented by the UZc, SH and the lowermost part of the UBS in UBSγ^3 (see Fig. 2). This volume is treated as one in the sections. In this model the SH is for simplicity assigned a volume of 0 km^3 [see the definition of the SH as a demarcation zone given by McBirney (1996)].

During construction of the NNW–SSE sections (Fig. 8), the extrapolation of the internal zone boundaries was sometimes found to overshoot control points and requires the introduction of post-solidification faults. Such faults are observed in the field and have been mapped (McBirney, 1989*b*). Most of the constructed faults correlate with faults identified in the field. The dip of the fault planes in the sections is the result of the angle between the section and the proposed fault plane and the orientation of the fault; these are therefore apparent dips. All the post-solidification faults are sub-parallel to the coast-parallel flexure (Nielsen & Brooks, 1981).

The schematic cross-sections of McBirney (1989*b*) and Irvine *et al.* (1998) show that the subdivisions of the MBS represent continuations of LS zones up along the walls of the intrusion. The zones and subzones in the UBS are the continuation of the same zones and subzones beneath the roof of the intrusion (Fig. 2). The exception is that no equivalents to UZc are mapped in the UBS or MBS.

The MBS increases in width with stratigraphic height in the LS (see, e.g. Hoover, 1989*a*, fig. 7). The transition between the LS and MBS can then be regarded as gradational and the boundaries between the LS, MBS

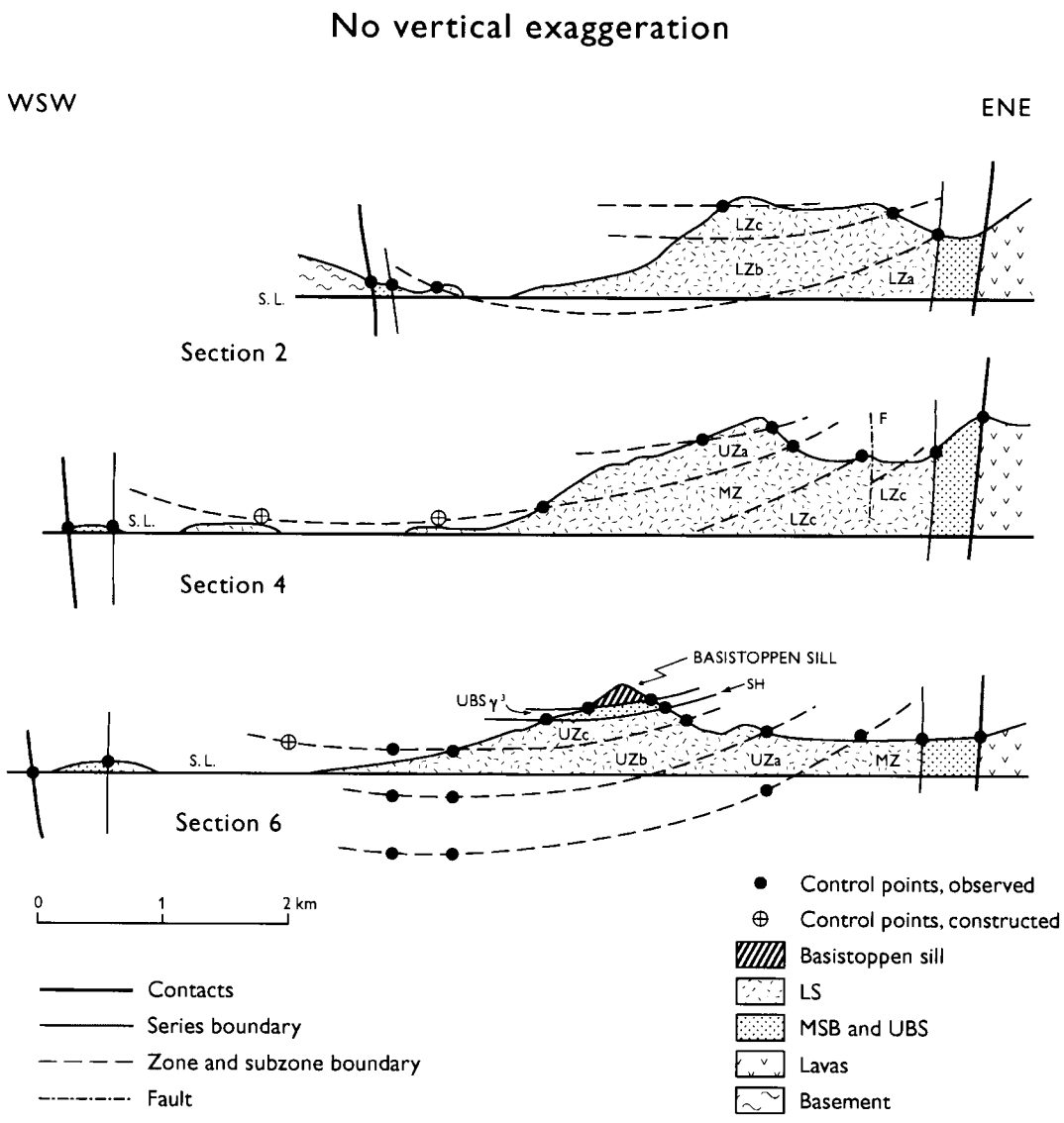

Fig. 7. ENE–WSW cross-sections (numbers 2, 4 and 6; see Fig. 1 and Electronic Appendices EA1.1 and EA1.2) constructed from the geological map (McBirney, 1989*b*) and drill-core data (Watts, Griffis & McOuat, 1991). Constructed control points have been projected onto the plane. Control points below the surface are from drill cores. Method and principles for the construction of the sections are described in the text. Lithological zones in the Layered Series (LS): HZ, Hidden Zone (only in Figs 8 and 9); LZa, Lower Zone a; LZb, Lower Zone b; LZc, Lower Zone c; MZ, Middle Zone; UZa, Upper Zone a; UZb, Upper Zone b; UZc, Upper Zone c; UBSγ^3, Upper Border Series gamma^3. S.L., sea level; MBS, Marginal Border Series; UBS, Upper Border Series. The important observation is the sagging of the boundaries between lithological zones in the centre of the intrusion. The sagging amounts to 700 m and an intrusion width of 7 km.

and UBS are, in a geochemical sense, artificial subdivisions of gabbros formed contemporaneously at crystallization fronts at the floor, on the walls and under the roof of the intrusion. The boundary between the LS, on the one hand, and the MBS and the UBS, on the other hand, is accordingly defined as a smooth plane. In the 2-D sections (Figs 8 and 9) the plane is represented by a line that runs from the contact at the base of the walls to the base of the UBS, in a trajectory that swings smoothly into the originally near-horizontal base of the UBS. The boundary between the UBS and the MBS is likewise a smooth line in the 2-D sections, and is the extension of the originally near-horizontal LS–UBS boundary (the Sandwich Horizon, SH) in the central part of the intrusion to the intersection between the steep walls and the roof of the intrusion.

Volume and mass proportions of the Skaergaard intrusion

The reconstructions (Figs 5, 8 and 9) are subject to significant uncertainties because of the limitations

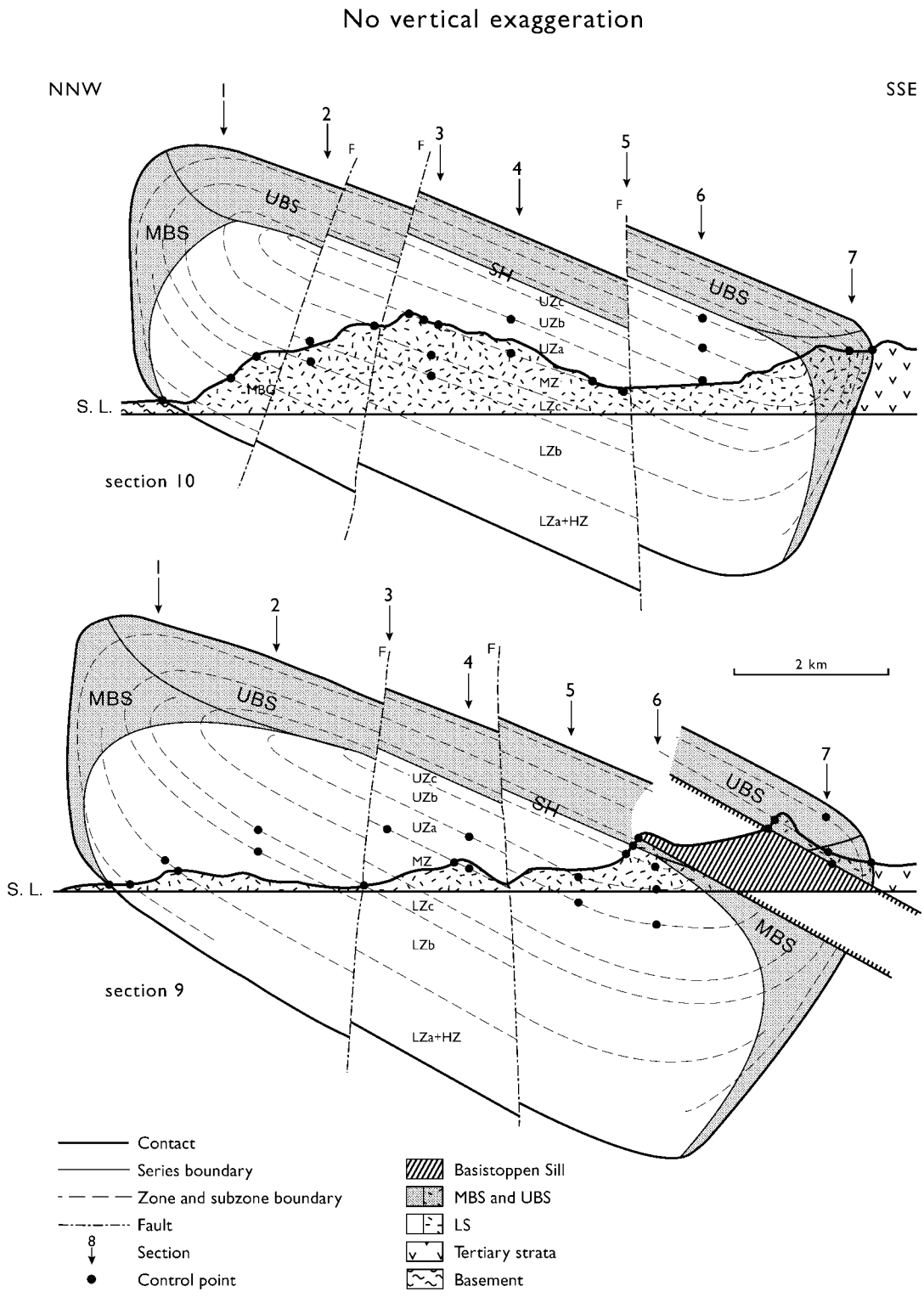

Fig. 8. NNW–SSE cross-sections (numbers 9 and 10; see Fig. 1) constructed from the geological map (McBirney, 1989*b*), the box model in Fig. 5, drill-core data (Watts, Griffis & McOuat, 1991) and the sections in Fig. 7 and Electronic Appendices EA1.1 and EA1.2. The sections show the proposed 'onion-skin' internal structure of the lithological zones in the Skaergaard intrusion. The methods and principles used for the construction of the sections are described in detail in the text. It is a basic assumption that the internal boundaries between lithological zones and subzones are isotherms and smooth. The numbered arrows show the location of the cross-sections in the grid in Fig. 1. Abbreviations as in Fig. 7. Further sections are shown in Electronic Appendix EA1.3.

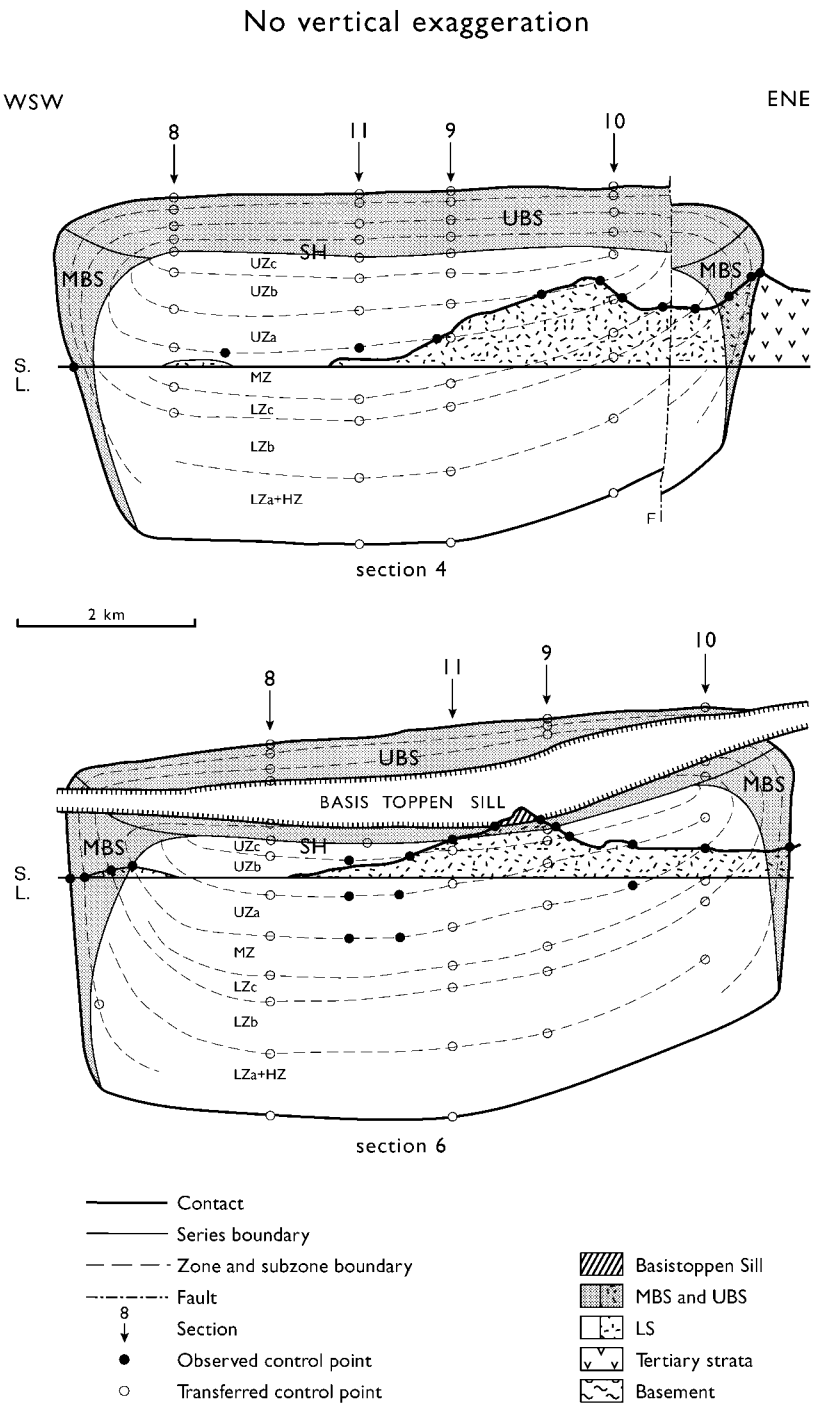

Fig. 9. Developed ENE–WSW cross-sections. The construction of the sections builds on the box model in Fig. 5, Fig. 7 and information obtained in Fig. 8. The model assumes an 'onion-skin' type structure (see Fig. 8). From Fig. 8, new control points are transferred that are created in the 'onion-skin' structure. (See legend for Fig. 8 and text.) Further sections are shown in Electronic Appendix EA1.3.

imposed by lack of field or other data; for example, in the SE and SW corners of the intrusion. The volume of the box has been calculated in four polygon models (Table 1; Electronic Appendices 2 and 3). All models assume an increase in the height of the magma chamber from 3·4 to 4·0 km from north to south as a result of the architecture of the coast-parallel flexure (Nielsen & Brooks, 1981).

Table 1: Estimates of volumes for the Skaergaard intrusion (details are given in Electronic Appendices 2 and 3)

	km^3
Bulk volume assuming height of magma chamber decreasing from 3·4 to 4·0 km from north to south, based on Fig. 5	
Tight multi-polygon model, approximation to contact	258·4
Tight polygon model assuming right-angle intersections between eastern, southern and western contacts	277·1
Two-polygon model (northern plus southern box)	274·5
One-polygon model assuming maximum north–south and east–west dimensions and average height of 3·7 km	302·5
Final volume estimates	280 ± 23
Maximum volumes of series as measured in Figs 8 and 9	
MBS	49·5
UBS	41·5
LS	211·2
Total (to be compared with one-polygon model)	302·2
Volumes of zones and subzones in LS as measured in Figs 8 and 9	
UZc	4·7
UZb	16·8
UZa	20·8
MZ	28·3
LZc	15·5
LZb	50·4
LZa including HZ	74·7
Total LS	211·2

The volume of the Skaergaard intrusion has been estimated in:

(1) a 'tight multi-polygon model' that follows the contacts very closely and in which the volume of each polygon is calculated by multiplying the area of the polygon by the average height in the polygon;
(2) the same 'tight multi-polygon model', but including the volumes of gabbro in the SE and SW corners assuming near-perpendicular intersections between the eastern, southern and western contacts;
(3) a simple 'two-polygon model' operating with a smaller northern and a larger southern box;
(4) a 'one-polygon model' based on maximum east–west and north–south dimensions and an average height of 3·7 km.

The estimated volumes vary from *c.* 260 to 300 km^3 (Table 1; Electronic Appendix 3). The volume of the Skaergaard intrusion is here estimated to be 280 ± 23 km^3 (± *c.* 8%), based on the average of the largest and smallest volume calculated in the models.

The volume proportions of series, zones and subzones in the LS can be estimated from the cross-sections (Figs 8 and 9). The inherent limitations in the modelling of the intrusion do not allow very precise estimates of the volumes. The maximum NNW–SSE, WSW–ENE length and width and the average height of zones and subzones are measured in the cross-sections and used for the volume calculation. The results are shown in Table 1. Details of the calculation can be found in Electronic Appendix 4. The sum of the calculated volumes of the LS, MBS and UBS should be comparable with the 'one-polygon model'. The calculation method overestimates the volumes of series, zones and subzones by approximately 8%, relative to the 'true' bulk volume of 280 km^3.

The volumes of the MBS and the UBS are calculated as for zones and subzones in the LS. The calculation assumes an average thickness of 600 m for the UBS and of 350 m for the MBS (see Figs 8 and 9). The volume of the UBS is calculated as the roof area multiplied by the average thickness of the UBS with a correction for overlap with the MBS at the intersection between the walls and the roof. The volume of the MBS is calculated as the area of the walls multiplied by the average thickness. The volume has been corrected for overlaps in the corners of the box and with the UBS at the top of the walls. The volume proportions of individual zones in the UBS and MBS are calculated assuming the same proportions in the UBS and MBS as in the equivalent LS zones (Electronic Appendix 3).

The volume of last crystallized melt that formed the lowermost UBS and uppermost LS on either side of the SH has been distributed to UZc of the LS and to UBSγ^3 in the volume proportions corresponding to the proportions of LS^{total} to UBS^{total}.

The sum of the zones and subzones of the LS, the MBS and the UBS is close to 300 km^3 (Table 1), similar to the 'one-polygon model'. Recalculated into percentages, the LS (including the HZ) represents 69·9%, UBS 13·7% and MBS 16·4% of the total volume. Within the LS the relative volume of the LZ (including the HZ) is 66·8%, MZ 13·5% and UZ 19·7%. The

Table 2: Volume to mass proportions for all zones and subzones of the Skaergaard intrusion

Zone or subzone	Volume (%)	Density	Mass proportion
LZa	24·79	3·07	23·97
MBS LZa	5·94	3·12	5·84
UBS alpha 1	4·89	3·02	4·65
LZb	16·73	3·16	16·65
MBS LZb	4·01	3·09	3·90
UBS alpha	3·30	3·04	3·16
LZc	5·14	3·36	5·44
MBS LZc	1·23	3·27	1·27
UBS alpha 2	1·01	3·05	0·97
MZ	9·39	3·31	9·79
MBS MZ	2·25	3·26	2·31
UBS beta	1·85	3·17	1·85
UZa	6·90	3·33	7·24
MBS UZa	1·65	3·31	1·72
UBS gamma 1	1·36	3·06	1·31
UZb	5·58	3·38	5·94
MBS UZb	1·34	3·00	1·27
UBS gamma 2	1·10	3·09	1·07
UZc	1·29	3·39	1·38
UBS gamma 3	0·27	3·29	0·28
SH	0·00	—	—

Volumes from Electronic Appendix 4; density calculated from norm in Electronic Appendix 5.

Table 3: Calculation of preferred parental Skaergard magma composition

	1 Initial bulk	2 Melano-granophyre	3 Initial bulk + 2% mgr.	4 Initial bulk + 5% mgr.	5 SK-TFDN parental SK melt
Concentrations in weight %					
SiO_2	46·86	62·18	47·17	47·63	47·91
TiO_2	3·09	1·07	3·05	2·99	3·09
Al_2O_3	13·44	12·41	13·42	13·39	13·80
FeO*	15·81	12·37	15·74	15·64	15·43
MnO	0·23	0·20	0·23	0·23	0·24
MgO	7·46	0·63	7·32	7·12	6·13
CaO	10·14	4·65	10·03	9·86	10·16
Na_2O	2·40	4·19	2·43	2·49	2·57
K_2O	0·31	1·99	0·34	0·39	0·40
P_2O_5	0·27	0·31	0·27	0·27	0·28
Mg number	0·49	0·09	0·48	0·48	0·45

mgr., melanogranophyre. All analyses recalculated to 100% volatile free and with all Fe as FeO. Mg number calculated assuming $Fe_2O_3/FeO = 0·15$. 1, Initial bulk composition for the Skaergaard magma with no corrections for melanogranophyre and Mg number correction (see text and Electronic Appendix 6). 2, Average melanogranophyre (McBirney, 1989*a*, table 8). 3, Preliminary Skaergaard bulk with 2% melanogranophyre (see text and Electronic Appendix 6). 4, Preliminary Skaergaard bulk cumulate with 5% melanogranophyre (see text and Electronic Appendix 6). 5, Preferred Skaergaard bulk (SK-TFDN). Column 4 after subtraction of 3% liquidus olivine Fo_{68} (see text and Electronic Appendix 6).

most noticeable feature of the estimate is the high volume proportion of the LZ (including the HZ), relative to the dominance of the MZ, UZ and UBS in surface exposures.

Mass balances for the intrusion require the transformation of the volume proportions into mass proportions. This has been achieved by calculating the average densities of the zones and subzones from the average cumulate compositions given by McBirney (1989*a*). The normative compositions have been transformed into densities using the CIPW normative mineral proportions and the densities of the appropriate mineral compositions (Deer *et al.*, 1971). This method for the calculation of densities has been adopted to avoid biases caused by the significant modal differences in the modal composition and density of individual samples of the often strongly layered gabbros. The mass proportions of zones and subzones are shown in Table 2 (details are given in Electronic Appendix 5).

The bulk composition of the intrusion

Previously calculated average compositions of the zones and subzones in the intrusion (McBirney, 1989*a*) and the mass proportions are used for the calculation of the bulk composition of the Skaergaard intrusion (Table 3; Electronic Appendix 6). For all zones and subzones in the LS bulk averages are used [All LZa, All LZb, etc., McBirney (1989*a*, tables 2–8)].

The calculated bulk composition (Table 3, column 1; see also details of the calculation in Electronic Appendix 6) does not include melanogranophyre. Melanogranophyre (Table 3, column 2) is common in UZb, UZc and in UBSγ[3]. Columns 3 and 4 in Table 3 show bulk compositions for the Skaergaard intrusion corrected by addition of 2 and 5% melanogranophyre, respectively. Melanogranophyre is here accepted as a comagmatic segregation. In exposures, the proportion of melanogranophyre does not seem to come close to 5%, but most of the upper zones that host melanogranophyre have been removed by erosion. The original

Table 4: Calculated trace element composition for the preferred parental magma of the Skaergaard intrusion and comparisons

	1 SK-TDFN parental SK melt	2 SK CM EG 4507	3 Average SK CM KT-39	4 High-Ti tholeiites G.P.Fm.	5 2nd cycle tholeiites G.P.Fm.	6 High-Ti tholeiite Skr.Fm.
Concentrations in ppm						
Ba	77	48	96	75	86	63
Li	7	n.d.	11	n.d.	n.d.	n.d.
Rb	8	6	15	7	4	7
Sr	241	285	240	254	227	194
Co	68	54	57	n.d.	51	51
Cr	89	330	199	185	65	84
Sc	37	23	35	35	39	38
Ni	80	120	141	99	66	66
Cu	265	118	105	243	287	332
Zn	133	69	191	117	140	134
Zr	128	93	159	175	192	168
La	10·67	5·6	6·8	n.d.	15·98	12·09
Sm	5·07	2·5	2·9	n.d.	6·79	6·23
Lu	0·380	0·19	0·20	n.d.	0·49	0·54

SK, Skaergaard intrusion; CM, chilled margin; EG, East Greenland; G.P.Fm., Geikie Plateau Formation; Skr.Fm., Skrænterne Formation; n.d., not determined. 1, Preferred parental magma of the Skaergaard intrusion calculated from the mass proportions (Table 2) and trace element concentrations (McBirney, 1989*a*, 1996). The composition includes 5% melanogranophyre and has been corrected by the subtraction of 3% liquidus olivine with 1300 ppm Ni (see Electronic Appendix 7). 2, Skaergaard chilled margin composition preferred by Wager (1960) [quoted from McBirney (1996, table 2)]. 3, Skaergaard KT-39 average chilled margin composition quoted from McBirney (1996, table 2). 4, Average of high-Ti tholeiites of the Geikie Plateau Formation, GGU 98512, 98513, 98516, 98464 and 98465 (Larsen *et al.*, 1989). 5, Average of high-Ti tholeiites of the Geikie Plateau Formation, second cycle of 'evolved tholeiites', GGU 435641–435644 and 435646–435647 (Andreasen, 2001). 6, Composition of high-Ti tholeiite lava (GGU 412481) in lower Skrænterne Formation (O. Stecher, personal communication, 2002).

proportion of melanogranophyre is thus not known. In addition, melanogranophyre is here taken as a proxy for all comagmatic felsic segregations in the intrusion.

The addition of melanogranophyre affects the bulk composition significantly by increasing SiO_2, high field strength elements (HFSE) and large ion lithophile elements (LILE) (see below). The composition with 2% melanogranophyre has a SiO_2 content of a little over 47%, which seems to be low compared with Tertiary East Greenland tholeiite compositions with similar Mg number (see Table 5, columns 4 and 9–12). The composition with 5% melanogranophyre has 47·6% SiO_2 and is preferred.

Modelling of the Skaergaard bulk magma composition assumes that the average compositions given by McBirney (1989*a*) are correct and representative. All samples used for the average composition of LZa (representing LZa + HZ in the present modelling) were collected in LZa close to the walls and the advancing cooling front. The samples used for the average composition of LZa cannot be representative of the 24% of the volume of the intrusion that is referred to LZa + HZ (Table 1). Slumps, relatively enriched in liquidus olivine, have descended along the cooling front and may have modified the compositions of most of the collected LZ samples.

Reduction in the MgO content and of the Mg number from 0·48 to 0·45 seems necessary to obtain equilibrium with liquidus olivine (Fo_{68}), similar to the most primitive olivine compositions recorded in the LS (McBirney, 1989*a*). A reduction in Mg number to 0·45 would also be in agreement with the contemporaneous plateau basalts with Mg numbers close to 0·45 that have liquidus olivine (Fo_{68}) (Larsen *et al.*, 1989). Olivine is the only one of the liquidus phases in LZa and LZb that can be used for a correction of the MgO content and the Mg number. The bulk composition in column 4 of Table 3 is corrected in column 5 to Mg number = 0·45 by the subtraction of 3% liquidus olivine (Fo_{68}). This bulk composition is believed to be a proxy for the parental magma that filled the Skaergaard intrusion, and in the following discussion is referred to as SK-TFDN.

The olivine correction of the bulk composition may well be valid because of the possible occurrence of gabbros in the unexposed, lower, parts of the intrusion that are more anorthositic than the LZa gabbros used for the calculation of the average LZa (McBirney, 1989*a*) [see also Irvine *et al.* (1998) for discussion]. Irrespective of these types of corrections, the Skaergaard bulk composition (Table 3, column 5) is an evolved, tholeiitic basalt with SiO_2 <48%; MgO <7%, Mg number *c.* 0·45; high FeO* and TiO_2, and FeO*/TiO_2 close to 5.

The trace element concentrations in SK-TFDN (Table 4 and Electronic Appendix 7) are modelled from the mass proportions in Table 2 and the average trace element compositions of zones and subzones of McBirney (1989*a*, 1996). The calculation of the trace element composition also assumes the addition of 5% melanogranophyre (McBirney, 1989*a*, table 8) and the subtraction of 3% liquidus olivine (Fo_{68}), with Ni estimated to be 1300 ppm (Hoover, 1989*a*). The proportion of melanogranophyre is important as LILE and HFSE are concentrated in the melanogranophyre. The trace element concentrations resemble those of

Table 5: Preferred parental major element composition (SK-TFDN) for the Skaergaard intrusion and comparison with other suggested parental compositions and Tertiary lavas in East Greenland

	1 SK-TFDN Parental SK melt	2 SK CM EG 4507	3 SK CM KT-39-1	4 SK CM average KT-39	5 CM SK dyke comp. C	6 EG MORB tholeiite	7 EG low-Ti tholeiite	8 EG med.-Ti tholeiite	9 EG high-Ti tholeiite	10 EG titano-tholeiite[1]	11 av. 2nd cycle G.P.Fm.	12 High-Ti tholeiite Skr.Fm.
Concentrations in wt %												
SiO_2	47·91	48·50	50·46	50·04	48·42	48·80	49·19	49·14	48·86	48·35	48·47	47·65
TiO_2	3·09	1·18	2·70	2·63	2·91	1·56	2·19	2·39	3·09	3·76	3·18	3·06
Al_2O_3	13·80	17·40	13·41	13·36	14·44	16·71	14·08	14·07	12·91	13·25	13·03	13·06
FeO*	15·43	9·73	12·96	13·14	13·71	11·22	12·39	12·88	15·24	14·13	15·39	15·65
MnO	0·24	0·16	0·22	0·22	0·21	0·18	0·19	0·23	0·23	0·19	0·24	0·25
MgO	6·13	8·71	6·71	7·29	6·38	7·31	7·27	7·34	5·80	6·28	5·86	6·43
CaO	10·16	11·50	10·34	10·22	10·70	11·91	12·17	11·24	10·71	10·82	10·77	10·73
Na_2O	2·57	2·39	2·41	2·41	2·46	2·06	2·10	2·24	2·47	2·41	2·39	2·55
K_2O	0·40	0·25	0·57	0·45	0·44	0·10	0·20	0·28	0·41	0·42	0·33	0·34
P_2O_5	0·28	0·1	0·22	0·22	0·32	0·13	0·20	0·19	0·28	0·38	0·31	0·28
Mg number	0·45	0·64	0·51	0·53	0·48	0·57	0·54	0·54	0·43	0·47	0·44	0·44
FeO^*/TiO_2	4·99	8·25	4·80	5·00	4·71	7·19	5·66	5·39	4·93	3·76	4·84	5·11

[1]Titano-tholeiite is a term introduced by Larsen *et al*. (1989) for tholeiitic lavas with $TiO_2 > 3{\cdot}5$ wt %.
SK, Skaergaard; CM, chilled margin; EG, East Greenland; G.P.Fm., Geikie Plateau Formation; Skr.Fm., Skrænterne Formation. Mg number calculated assuming $Fe_2O_3/FeO = 0{\cdot}15$. All analyses recalculated to 100% volatile free and with all Fe as FeO (FeO^*). 1, Preferred Skaergaard magma composition from Table 3. 2, Chilled margin sample EG 4507 from the Skaergaard intrusion preferred by Wager & Brown (1968), quoted from Hoover (1989*b*, table 9). 3, Chilled margin sample KT-39-1 from the Skaergaard intrusion preferred by Hoover (1989*b*, table 4). 4, Chilled margin average KT-39, the Skaergaard intrusion preferred by McBirney (1996, table 2). 5, Chill of Skaergaard-like dyke C from Brooks & Nielsen (1990, table 1). Composition preferred by Thy *et al*. (1995). 6, MORB-type tholeiite lava, Rømer Fjord Formation, GGU 96272, profile VII (Larsen *et al*., 1989). 7, Low-Ti tholeiite, Geikie Plateau Formation, GGU 98363, profile 47 (Larsen *et al*., 1989). 8, Medium-Ti tholeiite, Geikie Plateau Formation, GGU 98704, profile 59 (Larsen *et al*., 1989). 9, Skaergaard-like high-Ti tholeiite, Geikie Plateau Formation, GGU 98376, profile 47 (Larsen *et al*., 1989). 10, Titano-tholeiite, Geikie Plateau Formation, GGU 96942, profile 39 (Larsen *et al*., 1989). 11, Skaergaard-like high-Ti tholeiite, Geikie Plateau Formation, average of GGU 435641–435644 and 435646–435647 from Second Cycle of Geikie Plateau Formation (Andreasen, 2001). 12, Skaergaard-like high-Ti tholeiite from lower Skrænterne Formation, GGU 412481 (Danish Lithosphere Centre database).

common basaltic lavas and dykes in East Greenland (Table 4).

DISCUSSION

The box shape and emplacement mechanism

As argued by Irvine (1992) and Irvine *et al*. (1998), a box-like magma chamber is as dynamically reasonable as, or even more reasonable than, both the funnel-like (Wager & Brown, 1968) and the laccolith-like (Norton *et al*., 1984) geometries previously suggested. Without such faulting the intrusion might not have formed at all. The Skaergaard intrusion post-dates the initial tilting of the host rocks (Nielsen, 1978), but is itself tilted. This indicates that Skaergaard was emplaced during the flexuring of the East Greenland continental margin.

According to Nielsen & Brooks (1981), the formation of the coast-parallel flexure resulted from the collapse of the substructure of the continental margin as a result of magma pooling and extension. As also suggested by Irvine *et al*. (1998), the faulting resulted in the subsidence of the floor of the magma chamber to provide the space for the Skaergaard magma. That the floor subsided—rather than the roof being elevated—is found more plausible for the following reasons:

(1) the Skaergaard intrusion was emplaced in a tensional regime. A magma that would have had the buoyancy to lift a *c*. 2 km succession of lavas and several kilometres of Precambrian crust, up to 4 km, would probably have found its way through fault zones to the surface to extrude as a lava. A *c*. 2 km lid of Tertiary lavas has been estimated by Hirschmann *et al*. (1997).

Table 6: Comparison of percent crystallized in the Layered Series of the Skaergaard intrusion on the basis of stratigraphic height and mass proportions

	1	2	3
	Wager & Brown	Wager & Brown	This work
Based on:	Strat. height	Strat. height	Mass
HZ proportion:	60%	400 m	Incl. in LZa
Percent crystallized at base of indicated zone or subzone			
Top	100·0	100·0	100·0
UZc	96·6	92·8	98·2
Uzb	89·6	77·6	90·2
UZa	85·2	68·3	80·3
MZ	72·8	41·4	66·8
LZc	71·5	38·6	59·5
LZb	63·5	21·4	35·5
LZa	60·0	13·8	—
Base	0·0	0·0	0·0
Zone proportions			
UZ	14·8	31·7	19·7
MZ	12·4	26.9	13·5
HZ + LZ	72·8	41·4	66·8

(2) The lavas and sill formations are on strike with the successions south and east of the intrusion and do not suggest a significant lifting of the roof of the intrusion. At the south contact the roof of Skaergaard is located *c.* 1·5 km up into the lava succession, and this indicates a minimum subsidence of the floor of the intrusion of the order of 2·5 km.

(3) Had the floor below the Skaergaard intrusion not subsided, the roof over the intrusion would be composed of Precambrian basement and not Tertiary lavas, as indicated by the occurrence of rafts of lavas in the intrusion (see, e.g. Irvine *et al.*, 1998).

In contrast to the very extensive, contemporaneous, sills (Gisselø, 2000), the lateral movement of magma in the Skaergaard intrusion was inhibited on all sides by the fault planes. The accumulation of magma over an area restricted to *c.* 70 km^2 may have contributed to the subsidence of basement block below the intrusion.

The calculated SK-TFDN composition is not a primary mantle melt. The elevated initial Sr isotope ratio of the Skaergaard magma (Stewart & DePaolo, 1990) suggests tapping from a deep crustal magma chamber. The parental magma is, in agreement with Irvine *et al.* (1998), suggested to have moved from the deep feeder chamber to the upper-crustal magma chamber, while the basement block below the Skaergaard intrusion subsided. Such an emplacement mechanism would not have significantly affected the host rocks beyond the contacts of the intrusion.

The internal structure of the intrusion

It is a general assumption that all the magma emplaced into the magma chamber was retained in the intrusion. This is also suggested by the 'onion-skin' structure shown in the chemical sections of McBirney (1996). In these, geochemical data have been projected onto an east–west cross-section perpendicular to the dip of the intrusion. The sections that lend special support for the 'onion-skin' structure are those that show variations in the compositions of liquidus phases. The contouring of plagioclase (% An), pyroxene (Mg number) and olivine (Fo) liquidus compositions suggests that the most evolved liquids crystallized in the centre of the upper part of the intrusion (McBirney, 1996, fig. 11a–c). Other diagrams illustrate the variation in trace elements such as Ba and Ni (McBirney, 1996, fig. 11d and e). Ni is strongly correlated with the amount of olivine and does not reflect the sulphide content. The analysed sulphides from the intrusion are all Ni poor (Wager *et al*, 1957; Andersen *et al.*, 1998). The Ba variation generally shows an increase towards the upper central part of the magma chamber reflecting the increase in incompatible Ba in the residual melt. However, it should be noted that several excluded elements (e.g. Zr) do not show the 'onion-skin' distributions, possibly because of mobility of these elements during the late stages of solidification in the intrusion [see McBirney (2002) for discussion].

The last formed gabbros in the LS (UZc) are often interpreted as cumulates, but their texture is often more like granulite-facies rocks, showing well-developed corona textures and significant amounts of trapped granophyric melt (e.g. Wager & Deer, 1939). This texture could be taken as evidence for slow cooling and re-equilibration of the phases during the cooling and reaction between liquidus phases and retained fractions of melt in a closed system.

The volume

The volume of the intrusion was suggested by Wager & Brown (1968) to be *c.* 500 km^3. Norton *et al.* (1984) gave a volume of *c.* 170 km^3, which seems surprisingly low compared with the size of the intrusion, including the roots and the sill-like extensions (Fig. 6). An explanation for this could be that Norton *et al.* (1984)

described the intrusion to be *c.* 7 km × 4 km in surface exposure. These values are not correct, as the true size is 11 km × 8 km (Fig. 1). It is suspected that Norton *et al.* (1984) made their calculation in statute miles rather than kilometres. If this was the case their volume should be *c.* 500 km^3. This would be more consistent with the volume calculated here of 280 ± 23 km^3, which does not include the significant volumes in the roots and sill-like extensions included in the geophysical model. Single East Greenland lava flows have been demonstrated by Larsen *et al.* (1989) to have volumes up to 300 km^3.

Several workers have estimated the volume relationships between the LS, MBS and UBS. Naslund (1984) has estimated the volume proportion of the UBS to be 22% from the exposures in the southern part of the intrusion. He assumed a maximum thickness of the UBS of *c.* 900 m and an HZ equivalent to 12% of the total volume. In the present model the average thickness of the UBS is estimated at *c.* 600 m. The difference between the two estimates for the UBS may be explained by the 'onion-skin' structure. Parts of the UBS are only exposed close to the intersection between the southern wall and the roof of the intrusion, where fast cooling would have led to excessive thickness of UBS subzones. The currently suggested decrease in UBS thickness to <600 m under the more central parts of the roof cannot be verified as most of the UBS has been removed by erosion. Accepting the 'onion-skin' structure, a less extensive UBS volume must be assumed. With an average thickness of *c.* 600 m, the UBS is calculated to be *c.* 41·5 km^3 or *c.* 13·7 % of the original volume of magma.

The volume of the MBS is, as noted above, dependent on the preferred definition of the MBS. Following the definition given above, and as shown in the cross-sections (Figs 8 and 9), the MBS has been assigned an average width of 350 m and a total volume of 49·5 km^3 or 16·4% of the original volume of the intrusion.

In total, the LS will thus account for *c.* 70% of the initial magma volume including the small amount of magma chilled along the floor of the intrusion. This is in agreement with McBirney (1989*a*), who suggested a total for the UBS plus MBS of 30–40 vol. % (LS equivalent to 60–70 vol. %).

The geochemical variations in the LS of the Skaergaard intrusion are generally plotted against stratigraphic height (e.g. Wager & Brown, 1968). In most cases, the volume of remaining liquid has been equated to the proportion of the remaining stratigraphy, which requires that all zones originally had similar surface areas. In the original Wager & Deer (1939) and Wager & Brown (1968) models, the upper zones had increasing lateral extent and late-crystallized gabbros would then have had volume proportions exceeding the stratigraphic proportion. In the laccolith model of Blank & Gettings (1973) and Norton *et al.* (1984), the most evolved zones would have had volumes nearly proportional to their stratigraphic height. In the present model, the onion-skin structure would result in higher volume proportions for the earliest gabbros and lower volume proportions for the most evolved rocks compared with the stratigraphic proportions. Table 6 shows the proportion of crystallized melt at the base of the indicated zones and subzones in the LS in: (1) a model assuming 60% HZ and the stratigraphic columns given by Wager & Brown (1968); (2) a model assuming no more than 400 m of HZ (P. Thy, personal communication, 1998) and the stratigraphic column in Wager & Brown (1968); (3) the present mass proportion model.

It is important to note that the LZ + HZ volume of *c.* 70% required in the models of Wager & Deer (1939), Wager & Brown (1968) and Chayes (1970) seems to be satisfied in the present model, without assuming a large hidden volume of gabbros (Table 6). This is in accord with Brooks (1969) and Maaløe (1976), who did not support the existence of a major HZ.

The bulk composition

It would be surprising if a fully representative bulk composition for the Skaergaard intrusion could be calculated from the proposed mass proportions and the average compositions of zones and subzones given by McBirney (1989*a*, 1996, 2002). It is, however, believed that the calculated SK-TFDN major and trace element composition relates to specific geochemical types of contemporaneous lavas in the East Greenland plateau basalts (Tables 4 and 5). This is believed to give some credibility to the structural model and the calculated parental composition, and ties the Skaergaard intrusion into the regional magmatic evolution.

Major elements

The SK-TFDN composition (Table 3, column 5) is in accordance with the basaltic and tholeiitic nature of the intrusion. Support for the validity of the mass proportions used in the model is provided by the calculated P_2O_5 concentrations. The main reservoir for P in the intrusion is in cumulus apatite in UZb, the gabbros of which may have up to 4·45% P_2O_5 (McBirney, 1989*a*). The calculated bulk P_2O_5 of 0·27–0·28 wt % is very similar to the concentrations in the Fe- and Ti-rich contemporaneous plateau basalts with Mg number in the range 0·43–0·44 (Larsen *et al.*, 1989; Andreasen, 2001; Table 5). This is taken to support the suggested relative mass proportion between UZb and the bulk of the intrusion.

Table 7: Preferred parental Skaergaard magma compared with a composition based on stratigraphic proportions

	1	2
Model:	SK-TFDN Parental melt	Wager & Brown Strat. prop.
wt %		
SiO_2	47·91	47·01
TiO_2	3·09	3·63
Al_2O_3	13·80	12·58
FeO*	15·43	17·85
MnO	0·24	0·27
MgO	6·13	5·61
CaO	10·16	9·56
Na_2O	2·57	2·61
K_2O	0·40	0·44
P_2O_5	0·28	0·43
Mg number	0·45	0·39
FeO^*/TiO_2	4·99	4·92

Mg number calculated assuming $Fe_2O_3/FeO = 0·15$. All analyses recalculated to 100% volatile free and with all Fe as FeO. 1, SK-TFDN calculated on basis of mass proportions (Table 3, column 5). 2, 'Wager & Brown' composition assuming (a) mass proportional equivalent to stratigraphic height of exposed zones and subzones in Wager & Brown (1968); (b) HZ as in column 2 of Table 6; (c) addition of 5% granophyre.

Table 7 compares SK-TFDN with composition 'SK W + B' that is modelled from the stratigraphic proportions given by Wager & Brown (1968). SK W + B (Table 7, column 2) assumes an HZ of 400 m (P. Thy, personal communication, 1998) and includes 5% melanogranophyre. In the SK W+B composition the bulk P_2O_5 concentration would be as high as 0·43% and it is enriched in FeO* (17·85 wt %) and TiO_2 (3·63 wt %). The high concentration of these elements reflects an over-representation of the UZ zones in a model that equates stratigraphic height with mass proportion.

SK-TFDN is, in Table 5, compared with the major element compositions of the chilled margin of the intrusion (e.g. Wager & Deer, 1939; Wager & Brown, 1968; Hoover, 1989*b*) and contemporaneous dykes (Brooks & Nielsen, 1978, 1990). They have all been suggested to be proxies for the parental magma of the Skaergaard intrusion. Chilled margin sample EG 4507 (Table 5, column 2) was preferred by Wager (1960). It is an olivine tholeiite with an Mg number of 0·64 that does not agree with the earliest liquidus olivines (Fo_{68}) in the LS (McBirney, 1996) and in the MBS (Fo_{73}; Hoover, 1989*a*). EG 4507 also has an FeO^*/TiO_2 value of 8·25 compared with *c.* 5 in all other suggested Skaergaard compositions. EG 4507 cannot be a parental magma for the Skaergaard intrusion.

The KT-39-1 composition (Table 5, column 3) was preferred by Hoover (1989*b*). It shows many similarities to SK-TFDN, but has relatively elevated SiO_2 and K_2O and lower FeO*. The elevated SiO_2 and K_2O are believed to reflect mixing with granitic melt caused by thermal erosion along the contacts. An 'average KT-39' (average of three; McBirney, 1996; Table 5, column 4) shows, like KT-39-1, strong similarities to the parental magma composition preferred here, but also has high SiO_2. The Mg number is 0·53. The liquidus olivine would be Fo_{77} and the composition may be too Mg rich. Both KT-39 chilled margin compositions seem to be too SiO_2 rich compared with SiO_2 contents of around 48% in the regional, tholeiitic plateau basalts and dyke swarms (Table 5).

The composition of Skaergaard-like dyke C (Brooks & Nielsen, 1990; Table 4, column 5) is similar to SK-TFDN. The SiO_2 content seems more compatible with that of basaltic compositions from the plateau basalts in East Greenland (Table 5, columns 6–12), but the FeO* seems to be low and the Al_2O_3 high compared with SK-TFDN.

Examples of common types of tholeiites from the East Greenland plateau basalts (Table 5, columns 6–10; Larsen *et al.*, 1989; O. Stecher & C. Tegner, personal communication, 2002) are shown in order of increasing TiO_2. Mid-ocean ridge basalt (MORB), low-Ti and medium-Ti tholeiites [see definitions given by Larsen *et al.* (1989)] seem to be excluded as counterparts to SK-TFDN because of differences in Mg numbers (>0·5), TiO_2 concentrations (<2·80 wt % TiO_2) and FeO^*/TiO_2 (>5·4). TiO_2 content (>3·5 wt %) and FeO^*/TiO_2 (<4) also excludes titano-tholeiites. The only type of tholeiite comparable with SK-TFDN is a high-Ti tholeiite (Table 5; columns 9, 11 and 12). No other group of contemporaneous plateau basalts seem to have compositions with 2·8–3·3 wt % TiO_2, >15 wt % FeO*, FeO^*/TiO_2 around 5, and liquidus olivine (Fo_{68}) and plagioclase (An_{70}) (Larsen *et al.*, 1989, figs 46 and 52; Andreasen, 2001, pp. 23–29).

A closer inspection of the compositions of Tertiary East Greenland plateau basalts (Larsen *et al.*, 1989; Andreasen, 2001) and of the Danish Lithosphere Centre database for East Greenland plateau basalts (C. Tegner & O. Stecher, personal communication, 2002; Fig. 10) shows that SK-TFDN (Table 5, column 1) compares best with high-Ti tholeiite lavas in the uppermost part of the Geikie Plateau Formation (see Table 5, columns 9 and 11) and the lower part of the Skrænterne Formation [Table 5, column 12;

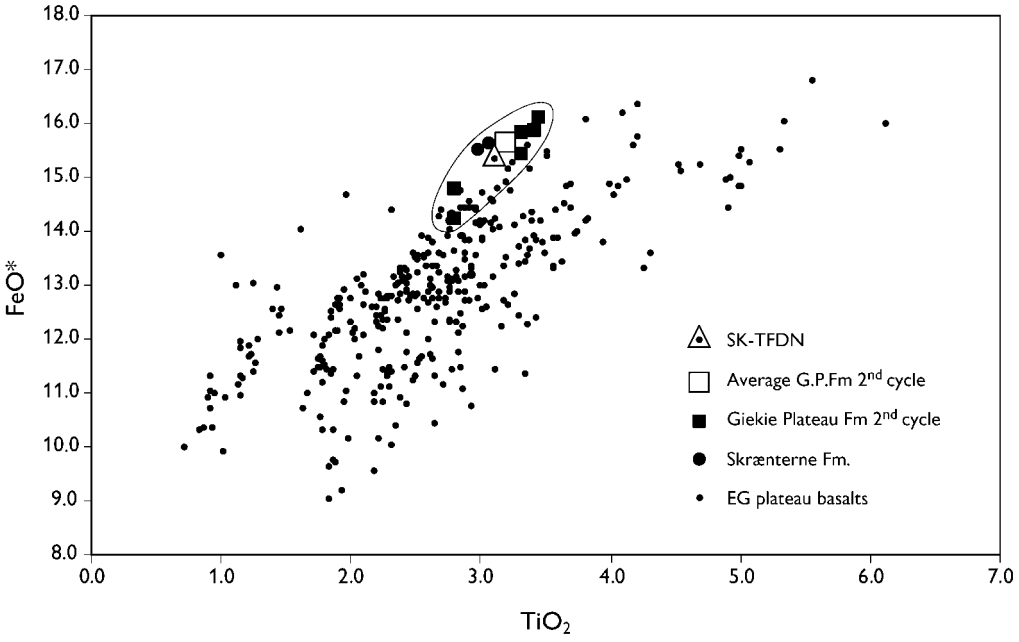

Fig. 10. FeO* vs TiO_2 variation for the 'Master Profile' (Danish Lithosphere Centre database) through the East Greenland plateau basalts. The preferred Skaergaard composition (SK-TFDN) belongs to a group of comparatively TiO_2-poor but FeO*-rich lavas (FeO*/TiO_2 wt % = 5) that includes HTS lavas from the Skrænterne Formation and a suite of HTS lavas in the upper part of the Geikie Plateau Formation. The latter are referred to the '2nd cycle evolved tholeiites' of the Geikie Plateau Formation, which are believed by Andreassen (2001) to represent a suite of related basaltic composition derived from a single waning volcanic system. All analyses recalculated to 100% volatile free with all Fe as FeO.

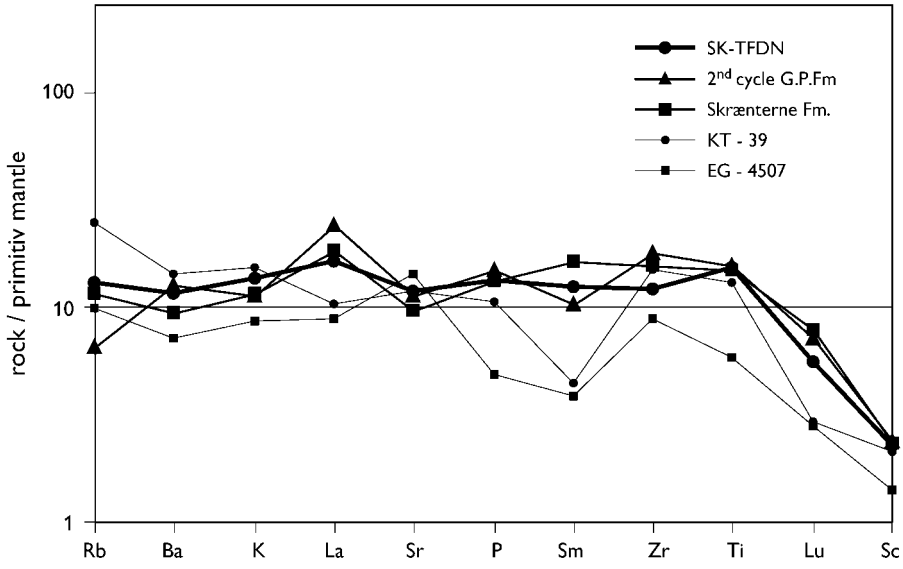

Fig. 11. Mantle-normalized trace element diagram for the calculated SK-TFDN composition and comparisons based on Table 4. The chilled margin samples (EG 4507 and KT-39) show negative anomalies in P and Sm. They are not likely magma compositions. SK-TFDN (modelled parental magma for the Skaergaard intrusion) compares well with the lava compositions from '2nd cycle evolved tholeiites' of the Geikie Plateau Formation and the Skrænterne Formation. Normalization according to values for primitive mantle given by McDonough & Sun (1995).

see Larsen *et al*. (1989) for details on the plateau basalts]. The composition in column 11 is the average of a suite of comagmatic high-Ti tholeiite lavas in the upper part of the Geikie Plateau Formation (Andreassen, 2001; see also Fig. 11).

Although SK-TFDN compares well with the evolved high-Ti tholeiites from upper Geikie Plateau Formation and lower Skrænterne Formation (Table 5), the estimates for Al_2O_3 and CaO may be in error. In SK-TFDN the Al_2O_3 content seems to be 0·5–1 wt %

too high and the CaO content is about 0·5 wt % too low compared with the high-Ti tholeiites. The reason for this discrepancy may be the previously mentioned bias in the LZa samples used for the bulk composition of LZa + HZ. Slumps at the base of the walls of the intrusion would add olivine and possibly plagioclase that was dragged along. An addition of olivine and plagioclase would relatively decrease the proportion of clinopyroxene. The net result would be a relative increase in Al_2O_3 and decrease in CaO. No good mode for a correction for this has been developed and the SK-TFDN composition has not been corrected further.

A correlation with lavas in the upper part of Geikie Plateau Formation or in the Skrænterne Formation corroborates the 55 Ma age of the Skaergaard intrusion (Hirschmann *et al*., 1997). The Tertiary plateau basalts formed between *c*. 57 and 53 Ma (Storey *et al*., 1996). The upper Geikie Plateau Formation and the lower Skrænterne Formation are located about two-thirds up the plateau basalt stratigraphy, equivalent to a succession of *c*. 2 km. An overburden of 2–3 km agrees with the syn-crystallization pressure estimate of *c*. 0·6 kbar in the SH (Lindsley *et al*., 1969; Hirschmann *et al*., 1997).

The parental magma of the Skaergaard intrusion seems to be common plateau basalt magma trapped in an upper-crustal reservoir. The magma was, as also suggested by Hoover (1989*b*), an evolved tholeiitic composition, and not an olivine tholeiite composition, as suggested by, for example, Wager & Deer (1939), Wager & Brown (1968) and Brooks & Nielsen (1978). The fact that SK-TFDN, despite all the uncertainties and assumptions, corresponds to compositions of known plateau basalt compositions lends support to the validity of the structural model and the calculated mass proportions of zones and subzones in the Skaergaard intrusion. It also supports the traditional view that the intrusion crystallized under closed-system conditions.

Trace elements

The trace element composition of SK-TFDN is given in Table 4 and Fig. 12 compared with Skaergaard chilled margin and Tertiary plateau basalts compositions.

The EG 4507 chilled margin composition (Table 4, column 2; Fig. 11) preferred by Wager (1960) [quoted from McBirney (1996)] has very high Cr compared with all other compositions in Table 4. In addition, it has low concentrations of a whole suite of elements, including Ba, La, Sm, Zr, Lu, Sc, Cu and Zn. This, and the prominent negative anomalies in P and Sm and low Zr, Lu and Sc, suggests that EG 4507 is not a likely parental composition for the Skaergaard intrusion.

A chilled margin average [KT-39; McBirney (1996); based on Hoover (1989*b*, table 10)] also has rather low La, Sm and Lu (Table 4, column 3; Fig. 11). The composition is [except for rare earth element (REE) concentrations] identical to the KT-AVG composition of Hoover (1989*b*, table 10, column 1). As for EG 4507, the negative Sm anomaly and high Rb and low Lu concentrations do not suggest the KT-39 average to be a good proxy for the parental magma of the Skaergaard intrusion.

Three compositions from the plateau basalts are shown in Table 4. Compared with the high-Ti tholeiite average in column 4, SK-TFDN is low in Cr and Zr. Chromite is a very rare phase in the cumulus olivine of LZa (Bollingberg, 1995). Minor concentrations of chromite cannot be excluded in the unexposed parts of the Skaergaard intrusion and would, if present, significantly increase the Cr concentrations in SK-TFDN. Significant variations in Zr are not easily explained, but may be caused by biases in the average compositions of McBirney (1989*a*, 1996), possibly as a result of the mobility of Zr and LREE during the late stages of crystallization of the Skaergaard magma [see McBirney (2002) for discussion]. The Geikie Plateau average (Table 4, column 5) is not included in Fig. 12 as REE are not included in the analysis.

SK-TFDN compares fairly well with the high-Ti tholeiite of the '2nd cycle evolved tholeiites' in the Geikie Plateau Formation (Andreasen, 2001) and high-Ti lava from the lower part of Skrænterne Formation (Table 4, columns 6 and 7; Fig. 11). Apart from comparatively high La and low Rb concentrations, the average of '2nd cycle evolved tholeiites' from the upper Geikie Plateau Formation and the high-Ti lava from the lower Skrænterne Formation compare closely with the SK-TFDN composition (Fig. 11). The '2nd cycle' average is slightly more evolved than SK-TFDN and this may explain the slightly elevated La in the '2nd cycle' average, whereas the low Rb is not explained.

The constant enrichment in SK-TFDN from Rb to Ti of 10–13 times relative to primitive mantle (Fig. 11) suggests that SK-TFDN may be a good proxy for the parental magma composition of Skaergaard.

Mass balance vs chilled margin compositions

No unique parental magma composition for the Skaergaard intrusion can be achieved by mass balance calculations. Although the database for such calculations is extensive, many choices and evaluations have to be made. The compositions of the chilled margins in Tables 4 and 5, and the detailed investigation of Hoover (1898*b*), show how difficult it is to select a specific sample as *the* representative sample of the parental magma. In detail, the chilled margin compositions vary significantly (Hoover, 1989*b*), as a result of wall-rock contamination and accumulation effects.

It is, however, argued that the mass balance approach is a valid alternative method, which allows selection of lavas, dykes and possibly also chilled margin samples that could have compositions close to that of the parental magma of the Skaergaard intrusion. It must, however, be emphasized that all lava and probably also all dyke compositions that may be compared with the parental composition of the Skaergaard intrusion equilibrated and differentiated in crustal magma chambers. They may all have unique characteristics, and no lava or dyke may in all details represent the parental magma of the Skaergaard intrusion.

CONCLUSIONS

The number of uncertainties, such as lack of information on the shape and orientation of the contacts at depth, lack of information on the depth to the floor, the possible biases in average compositions, the mobility of excluded elements, etc., limit the accuracy with which a bulk composition for the Skaergaard intrusion can be calculated. It is, however, considered that a 'box and onion-skin model' is a valid model for the Skaergaard intrusion because of its simplicity, the simple dynamics of magma emplacement, and because the model allows the calculation of realistic parental magma composition for the Skaergaard intrusion.

It is suggested that:

(1) the Skaergaard intrusion is a fault-controlled, box-like intrusive body emplaced about 55 Myr ago within a fault block of the extended and thinned East Greenland continental margin. The magma was emplaced with a roof at an original depth of *c*. 2 km. The floor subsided to provide room for the magma.
(2) The intrusion is *c*. 11 km north–south, up to 8 km east–west and up to 4 km deep. The volume is *c*. 280 km^3, comparable with that of the large contemporaneous lava flows.
(3) Cooling from the walls, roof and floor in combination with accumulation on the floor resulted in an 'onion-skin' internal structure and accumulation of late, low-temperature magma in the upper central part of the magma chamber.
(4) Only a small proportion of the stratigraphic column is not exposed, as a result of southward tilting of the intrusion and the level of erosion.
(5) Disagreement between early models suggesting a voluminous and deep HZ and more recent geochemical and geophysical models suggesting a restricted HZ seems to be an artefact of unresolved volumetric relations for lithological zones and subzones in the Skaergaard intrusion.
(6) The bulk composition of the intrusion is that of a high-Ti tholeiite, comparable with those of contemporaneous flood basalts in the upper part of the Geikie Plateau or lower Skrænterne Fomation, formed at the East Greenland continental margin during the opening of the North Atlantic.
(7) The onion-skin structure of the Skaergaard intrusion suggests that it cooled and crystallized under generally closed-system conditions.

ACKNOWLEDGEMENTS

The results published in this paper are published with the permission of the Geological Survey of Denmark and Greenland. Ole Stecher (Danish Lithosphere Centre) helped to prepare Fig. 11. Per Gisselø supplied the photograph in Fig. 5. C. Kent Brooks, Brian Upton, Peter Thy and Chip (C. E.) Lesher are thanked for many valuable suggestions and discussions. Excellent reviews by A. R. McBirney, S. A. Morse, C. Tegner, R. G. Cawthorn and M. Wilson are highly appreciated.

SUPPLEMENTARY DATA

Supplementary data for this paper are available on *Journal of Petrology* online.

REFERENCES

Andersen, J. C. Ø., Rasmussen, H., Nielsen, T. F. D. & Rønsbo, J. G. (1998). The Triple Group and the Platinova gold and palladium reefs in the Skaergaard intrusion: stratigraphic and petrographic relations. *Economic Geology* **93**, 488–509.

Andreasen, R. (2001). Cyclical compositional variations in the Geikie Plateau Formation of the Palaeogene flood basalts, east Greenland: inferences about magma chamber processes. M.Sc. thesis, University of Copenhagen, 179 pp.

Bird, D. K., Brooks, C. K., Gannicott, R. A. & Turner, P. A. (1991). A gold-bearing horizon in the Skaergaard intrusion, East Greenland. *Economic Geology* **86**, 1083–1092.

Blank, H. R. & Gettings, M. E. (1973). Subsurface form and extent of the Skaergaard intrusion, East Greenland (abstract). *EOS Transactions, American Geophysical Union* **54**, 507.

Blickert-Toft, J., Lesher, C. E. & Rosing, M. T. (1992). Selectively contaminated magmas of the Tertiary East Greenland macrodike complex. *Contributions to Mineralogy and Petrology* **110**, 154–172.

Bollingberg, K. (1995). Textural and chemical evolution of the Fe–Ti oxide minerals during late- and post magmatic cooling of the Skærgaard intrusion, East Greenland. M.Sc. thesis, University of Copenhagen, 149 pp.

Brooks, C. K. (1969). On the distribution of zirconium and hafnium in the Skaergaard intrusion, east Greenland. *Geochimica et Cosmochimica Acta* **33**, 357–374.

Brooks, C. K. & Gleadow, A. J. W. (1977). A fission track age for the Skaergaard intrusion and the age of the east Greenland basalts. *Geology* **5**, 539–540.

Brooks, C. K. & Nielsen, T. F. D. (1978). Early stages of the Skaergaard magma as revealed by a closely related suite of dike rocks. *Lithos* **11**, 1–14.

Brooks, C. K. & Nielsen, T. F. D. (1982*a*). The E Greenland continental margin: a transition between oceanic and continental magmatism. *Journal of the Geological Society, London*, **139**(3), 265–275.

Brooks, C. K. & Nielsen, T. F. D. (1982*b*). The Phanerozoic development of the Kangerdlugssuaq area, East Greenland. *Meddelelser om Grønland, Geoscience* **9**, 30 pp.

Brooks, C. K. & Nielsen, T. F. D. (1990). The differentiation of the Skaergaard intrusion. A discussion of R. H. Hunter & R. S. J. Sparks (Contrib. Mineral. Petrol. 95: 451–461). *Contributions to Mineralogy and Petrology* **104**, 244–247.

Chayes, F. (1970). On estimating the magnitude of the Hidden Zone and the compositions of the residual liquids of the Skaergaard Layered Series. *Journal of Petrology* **11**, 1–14.

Deer, W. A., Howie, R. A. & Zussman, J. (1971). *An Introduction to the Rock-forming Minerals*. Harlow: Longman.

Gisselø, P. (2000) Sorgenfri Gletscher Sill Complex, East Greenland. Solidification mechanisms of sheet-like bodies and the role of sill complexes in large igneous provinces. Ph.D. thesis, Aarhus University, 100 pp.

Hirschmann, M. M., Renne, P. R. & McBirney, A. R. (1997). ^{40}Ar/^{39}Ar dating of the Skaergaard intrusion. *Earth and Planetary Science Letters* **146**, 645–658.

Hoover, J. D. (1989*a*). Petrology of the Marginal Border Series of the Skaergaard intrusion. *Journal of Petrology* **30**, 399–439.

Hoover, J. D. (1989*b*). The chilled margin gabbro and other contact rocks of the Skaergaard intrusion. *Journal of Petrology* **30**, 441–476.

Hunter, R. H. & Sparks, R. S. J. (1987). The differentiation of the Skaergaard intrusion. *Contributions to Mineralogy and Petrology* **95**, 451–461.

Irvine, T. N. (1987). Layering and related structures in the Duke Island and Skaergaard intrusions: similarities, differences and origins. In: Parsons, I. (ed.) *Origins of Igneous Layering. NATO ASI Series C* **196**, 185–245.

Irvine, T. N. (1992). The emplacement of the Skaergaard intrusion. *Carnegie Institution of Washington Yearbook* **91**, 91–96.

Irvine, T. N., Andersen, J. C. Ø. & Brooks, C. K. (1998). Included blocks (and blocks within blocks) in the Skaergaard intrusion, East Greenland. *Geological Society of America Bulletin* **110**(11), 1398–1447.

Kays, M. A., Goles, G. G. & Grover, T. W. (1989). Precambrian sequence bordering the Skaergaard intrusion. *Journal of Petrology* **30**, 321–361.

Larsen, L. M., Watt, W. S. & Watt, M. (1989). Geology and petrology of the Lower Tertiary plateau basalts of the Scoreby Sund region, East Greenland. *Bulletin of Grønlands Geologiske Undersøgelse* **157**, 164 pp.

Larsen, M., Bjerager, M., Nedkvitne, T., Olaussen, O. & Preuss, T. (2001). Pre-basaltic sediments (Aptian–Paleocene) of the Kangerlussuaq Basin, southern East Greenland. *Geology of Greenland Survey Bulletin* **189**, 99–106.

Lesher, C. E., Thy, P. & Jackson, H. (1993). Origin of fine-scale igneous layering in gabbroic rocks of the Miki Fjord macrodike intrusion. *EOS Transactions, American Geophysical Union* **74**, 623.

Lindsley, D. H., Brown, G. M. & Muir, I. D. (1969). Conditions of the ferrowollastonite–ferrohedenbergite inversion in the Skaergaard intrusion, East Greenland. *Mineralogical Society of America, Special Paper* **2**, 193–201.

Maaløe, S. (1976). The zoned plagioclase of the Skaergaard intrusion, East Greenland. *Journal of Petrology* **17**, 318–419.

McBirney, A. R. (1989*a*). The Skaergaard Layered Series: I. Structure and average compositions. *Journal of Petrology* **30**, 363–397.

McBirney, A. R. (1989*b*). Geological map of the Skaergaard intrusion, east Greenland. Eugene: University of Oregon.

McBirney, A. R. (1996). The Skaergaard intrusion. In: Cawthorn, R. G. (ed.) *Layered Intrusions*. Amsterdam: Elsevier, pp. 147–180.

McBirney, A. R. (2002). The Skaergaard Layered Series. Part VI. Excluded elements. *Journal of Petrology* **43**, 535–556.

McBirney, A. R. & Naslund, H. R. (1990). The differentiation of the Skaergaard intrusion. A discussion of R. H. Hunter and R. S. J. Sparks (Contrib. Mineral. Petrol. 95: 451–461). *Contributions to Mineralogy and Petrology* **104**, 235–240.

McBirney, A. R. & Noyes, R. M. (1979). Crystallization and layering in the Skaergaard intrusion. *Journal of Petrology* **20**, 487–554.

McDonough, W. F. & Sun, S.-s. (1995). The composition of the Earth. *Chemical Geology* **120**(3–4), 223–253.

Morse, S. A. (1990). The differentiation of the Skaergaard intrusion. A discussion of R. H. Hunter and R. S. J. Sparks (Contrib. Mineral. Petrol. 95: 451–461). *Contributions to Mineralogy and Petrology* **104**, 240–244.

Naslund, H. R. (1984). Petrology of the Upper Border Series of the Skaergaard intrusion. *Journal of Petrology* **25**, 185–212.

Nielsen, T. F. D. (1975). Possible mechanism of continental break-up in the North Atlantic. *Nature* **253**, 182–184.

Nielsen, T. F. D. (1978). The Tertiary dike swarms of the Kangerdlugssuaq area, East Greenland. An example of magmatic development during continental break-up. *Contributions to Mineralogy and Petrology* **67**, 63–78.

Nielsen, T. F. D. (1987). Tertiary alkaline magmatism in East Greenland: a review. In: Fitton, J. G. & Upton, B. G. J. (eds) *Alkaline Igneous Rocks. Geological Society, London, Special Publications* **30**, 489–515.

Nielsen, T. F. D. (2001). The palladium potential of the Skaergaard intrusion, South-East Greenland. *Report GEUS* **2001/23**, 38 pp.

Nielsen, T. F. D. & Brooks, C. K. (1981). The East Greenland rifted continental margin; an examination of the coastal flexure. *Journal of the Geological Society, London* **138**(5), 559–568.

Nielsen, T. F. D. & Schønwandt, H. K. (1990). Gold and platinum group metal mineralisation in the Skaergaard intrusion, southern east Greenland. *Grønlands Geologiske Undersøgelse Rapport* **148**, 101–103.

Nielsen, T. F. D., Soper, N. J., Brooks, C. K., Faller, A. M., Higgins, A. C. & Matthews, D. W. (1981). The pre-basaltic sediments and the Lower Basalts at Kangerdlugssuaq, East Greenland: their stratigraphy, lithology, palaeomagnetism and petrology. *Meddelelser om Grønland, Geoscience* **6**, 25 pp.

Norton, D., Taylor, H. P., Jr & Bird, D. K. (1984). The geometry and high-temperature brittle deformation of the Skaergaard intrusion. *Journal of Geophysical Research* **89B**, 10178–10192.

Pedersen, A. K., Watt, M., Watt, W. S. & Larsen, L. M. (1997). Structure and stratigraphy of early Tertiary basalts of the Blosseville Kyst, East Greenland. *Journal of the Geological Society, London* **154**(3), 565–570.

Rosing, M. T., Lesher, C. E. & Bird, D. K. (1989). Chemical modification of East Greenland Tertiary magmas by two-liquid interdiffusion. *Geology* **17**, 626–629.

Stewart, B. W. & DePaolo, D. J. (1990). Isotopic studies of processes in mafic magma chambers; II The Skaergaard intrusion, East Greenland. *Contributions to Mineralogy and Petrology* **104**, 125–141.

Storey, M., Pedersen, A. K., Larsen, H. C., Larsen, L. M., Stecher, O., Duncan, R. A., Tegner, C. & Carlson, R. W. (1996). Middle Miocene volcanism in East Greenland. *EOS Transactions, American Geophysical Union* **77**(46), F823.

Tegner, C., Lesher, C. E., Larsen, L. M. & Watt, W. S. (1998). Evidence from the rare-earth element record of mantle melting for cooling of the Tertiary Iceland plume. *Nature* **395**, 591–594.

Thy, P., Lesher, C. E., Nielsen, T. F. D. & Brooks, C. K. (1996). Experimental modelling of Skaergaard cumulates. *EOS Transactions, American Geophysical Union* **77**(46), F822.

Toplis, M. J. & Carroll, M. R. (1995). An experimental study of the influence of oxygen fugacity on Fe–Ti oxide stability, phase relations, and mineral–melt equilibria in ferro-basaltic systems. *Journal of Petrology* **36**, 1137–1170.

Turner, P. A. (1990). Report of the 1989 field season—Skaergaard concession. Unpublished report, Platinova Resources Ltd.–Corona Corporation Joint Venture, Toronto, Ont. (in the archives of the Geological Society of Denmark and Greenland, GEUS Report File 20843), 47 pp.

Wager, L. R. (1947). Geological investigations in East Greenland. Part IV, The stratigraphy and tectonics of Knud Rasmussens Land and the Kangerdlugssuaq region. *Meddelelser om Grønland* **134**(3), 64 pp.

Wager, L. R. (1960). Major and trace element variation of the Layered Series of the Skaergaard Intrusion and a re-estimate of the average composition of the Hidden Layered Series and of the successive residual magmas. *Journal of Petrology* **1**, 364–398.

Wager, L. R. & Brown, G. M. (1968). *Layered Igneous Rocks*. Edinburgh: Oliver & Boyd.

Wager, L. R. & Deer, W. A. (1939). Geological investigations in east Greenland. Part III. The petrology of the Skaergaard intrusion, Kangerdlugssuaq, East Greenland. *Meddelelser om Grønland* **105**(4), 352 pp.

Wager, L. R., Vincent, E. A. & Smales, A. A. (1957). Sulphides in the Skaergaard intrusion, east Greenland. *Economic Geology* **52**, 855–903.

Watts, Griffis & McOuat (1991). Appendix II, Summary of 1990 Skaergaard samples by hole and type. In: Watts, Griffis & McOuat (eds) *1990 Skaergaard Project, Platinova/Corona Concession, East Greenland 2A*. Toronto, Ont: Watts, Griffis & McOuat (in archives of the Geological Survey of Denmark and Greenland, GEUS Report File 20848), pp. 71–165.

White, C. M., Geist, D. J., Frost, C. D. & Verwoerd, W. J. (1989). Petrology of the Vandfaldsdalen Macrodike, Skaergaard Region, east Greenland. *Journal of Petrology* **30**, 271–299.